Development/Plasticity/Repair

miR-218 Promotes Dopaminergic Differentiation and Controls Neuron Excitability and Neurotransmitter Release through the Regulation of a Synaptic-Related Genes Network

Salvatore Pulcrano,[1] Roberto De Gregorio,[1,2] Claudia De Sanctis,[1,3] Floriana Volpicelli,[1,4] Rosa Maria Piscitelli,[5] Luisa Speranza,[6] Carla Perrone-Capano,[1,4] Umberto di Porzio,[1] Massimiliano Caiazzo,[7,8] Alessandro Martini,[5] Cecilia Giacomet,[5] Diego Medina,[9,10] Rajeshwar Awatramani,[11] Davide Viggiano,[12] Mauro Federici,[5] Nicola B. Mercuri,[5,13] Ezia Guatteo,[5,14] and Gian Carlo Bellenchi[1,5]

[1]Institute of Genetics and Biophysics, Consiglio Nazionale delle Ricerche, Naples, 80131, Italy, [2]Caryl and Israel Englander Institute for Precision Medicine, Weill Cornell Medicine and New York Presbyterian, New York, New York 10021, [3]Neuropathology Brain Bank at Mount Sinai, New York, New York 10029, [4]Department of Pharmacy, School of Medicine and Surgery, University of Naples Federico II, Naples, 80131, Italy, [5]Fondazione Santa Lucia Istituto Di Ricovero e Cura a Carattere Scientifico, Rome, 00143, Italy, [6]Dominick P. Purpura Department of Neuroscience, Albert Einstein College of Medicine, New York, New York 10461, [7]Department of Molecular Medicine and Medical Biotechnology, University of Naples Federico II, Naples, 80131, Italy, [8]Department of Pharmaceutics, Utrecht Institute for Pharmaceutical Sciences, Utrecht University, Utrecht, 3584 CG, The Netherlands, [9]Telethon Institute of Genetics and Medicine, Pozzuoli, 80078, Italy, [10]Department of Medical and Translational Science, Federico II University, Naples, 80131, Italy, [11]Department of Neurology at Northwestern University Chicago, Illinois 60611, [12]Department of Translational Medical Sciences, University of Campania "L. Vanvitelli," Naples, 80131, Italy, [13]University of Tor Vergata, Department of Systems Medicine, Rome, 00133, Italy, and [14]Department of Motor Science and Wellness, Parthenope University, Naples, 80133, Italy

In the brain, microRNAs (miRNAs) are believed to play a role in orchestrating synaptic plasticity at a higher level by acting as an additional mechanism of translational regulation, alongside the mRNA/polysome system. Despite extensive research, our understanding of the specific contribution of individual miRNA to the function of dopaminergic neurons (DAn) remains limited. By performing a dopaminergic-specific miRNA screening, we have identified miR-218 as a critical regulator of DAn activity in male and female mice. We have found that miR-218 is specifically expressed in mesencephalic DAn and is able to promote dopaminergic differentiation of embryonic stem cells and functional maturation of transdifferentiated induced DA neurons. Midbrain-specific deletion of both genes encoding for miR-218 (referred to as miR-218-1 and mir218-2) affects the expression of a cluster of synaptic-related mRNAs and alters the intrinsic excitability of DAn, as it increases instantaneous frequencies of evoked action potentials, reduces rheobase current, affects the ionic current underlying the action potential after hyperpolarization phase, and reduces dopamine efflux in response to a single electrical stimulus. Our findings provide a comprehensive understanding of the involvement of miR-218 in the dopaminergic system and highlight its role as a modulator of dopaminergic transmission.

Key words: **conditional KO; dopamine; excitability; miR-218; miRNAs; substantia nigra**

Received Mar. 8, 2023; revised July 25, 2023; accepted Aug. 10, 2023.

Author contributions: S.P., R.D.G., C.D.S., U.d.P., A.M., C.G., D.M., R.A., M.F., N.B.M., E.G., and G.C.B. designed research; S.P., R.D.G., C.D.S., F.V., R.M.P., L.S., C.P.-C., U.d.P., M.C., A.M., C.G., D.M., R.A., D.V., M.F., N.B.M., E.G., and G.C.B. performed research; S.P., R.D.G., C.D.S., F.V., R.M.P., L.S., C.P.-C., U.d.P., M.C., A.M., C.G., D.M., R.A., D.V., M.F., N.B.M., E.G., and G.C.B. analyzed data; S.P. and R.D.G. wrote the first draft of the paper; S.P., R.D.G., and G.C.B. edited the paper; S.P., C.P.-C., U.d.P., M.C., A.M., C.G., R.A., M.F., N.B.M., E.G., and G.C.B. wrote the paper.

This work was supported by Programmi di Ricerca Scientifica di Rilevante Interesse Nazionale. PRIN 2017T9JNLT_004 and P2022K5PTK to G.C.B.; Ricerca Interdisciplinare DM737 to E.G.; National Institutes of Health R01NS119690 to R.A.; Telethon Foundation TMDMMFU22TT to D.M.; and MUR-NRRP Project MNESYS PE0000006 to C.P.-C. We thank the High Content Screening Facility at Telethon Institute of Genetics and Medicine for support with the microRNA screening.

The authors declare no competing financial interests.

Correspondence should be addressed to Gian Carlo Bellenchi at giancarlo.bellenchi@igb.cnr.it.

https://doi.org/10.1523/JNEUROSCI.0431-23.2023

Significance Statement

In the past decade, several miRNAs have emerged as potential regulators of synapse activity through the modulation of specific gene expression. Among these, we have identified a dopaminergic-specific miRNA, miR-218, which is able to promote dopaminergic differentiation and regulates the translation of an entire cluster of synapse related mRNAs. Deletion of miR-218 has notable effects on dopamine release and alters the intrinsic excitability of dopaminergic neurons, indicating a direct control of dopaminergic activity by miR-218.

Introduction

The contribution of microRNAs (miRNAs) to neuronal function remains a major challenge in neuroscience. MicroRNAs (miRNAs) are small noncoding single-strand RNA (19-22 nucleotides) acting as post-transcriptional regulators of gene expression. They bind to 6-8 bp miRNA-recognition elements, located at the 3′-untranslated regions (UTRs) of target mRNAs resulting in either mRNA cleavage or inhibition of translation (Bartel, 2004). Their physiological role has remained evasive, mostly because of the high number and the endless combinations of miRNA(s)-mRNA(s) pairing. miRNA-mRNA binding affinity may vary depending on various factors, including differences in their expression levels, adding a further layer of complexity to any functional prediction. While an miRNA recognizes and binds the same miRNA-recognition elements on different mRNAs, each mRNA hosts multiple miRNA-recognition elements recognized by different miRNAs at its 3′UTR. This complexity makes it difficult to predict the effective biological relevance of a miRNA-mRNA interaction *in vivo*. Additionally, miRNA families with similar seed sequences create functional redundancy, making it difficult to determine the importance of individual miRNAs as recently shown for the miR-34/449 (Chang et al., 2021).

The involvement of miRNAs in the mesencephalic dopaminergic neurons (DAn) has been largely studied for their possible role in the etiopathogenesis of Parkinson's disease. Knocking out the key miRNA biosynthetic enzyme Dicer results in a morphologic aberrant phenotype characterized by the failure of DAn differentiation (Huang et al., 2010). Similarly, in adult animals, decreased Dicer expression in the substantia nigra (SN) is associated with motor learning impairment and progressive neuronal degeneration (Pang et al., 2014). This suggests that miRNAs may have a role in the regulation of the adult DAn system plasticity through the modulation of individual synapse activity through local translational control (Martin and Ephrussi, 2009; Colameo et al., 2021). However, which specific miRNAs contribute to the physiological regulation of DAn remain unclear. Among these miR-218, a motor neuron-related miRNA has been associated with DAn because of its expression in the midbrain during embryonic development (Huang et al., 2010) and its capability to facilitate astrocyte to DAn conversion in a Parkinson's disease model (di Val Cervo et al., 2017). However, how miR-218 impacts the neurophysiological characteristics and functions of DAn *in vivo* has not been elucidated yet.

In the genome, miR-218 is present in two identical copies, named miR218-1 and miR218-2, located intronically in the Slit2 and Slit3 genes, respectively. Deletion of both isoforms results in perinatal lethality apparently associated with motor neurons synaptogenesis defects (Amin et al., 2015), and rare human miR-218 gene variants, with reduced miR-218 expression, have been identified in amyotrophic lateral sclerosis patients (Reichenstein et al., 2019). Changes in miR-218 expression have been linked to neurodegenerative and neuropsychiatric disorders, including Alzheimer's disease, Parkinson's disease, schizophrenia, depression, or anxiety, overall suggesting a basic role in the proper physiology of different neuronal subtypes (Reichenstein et al., 2019; Torres-Berrío et al., 2020).

The relationship between miR-218 and its targets has been challenging to predict and appears to depend on several unidentified factors, as changes in miR-218 expression levels result in an unexpected regulation of distinct gene networks (Amin et al., 2021). Multiple lines of evidence point to miR-218 as an important player in a complex set of processes associated with the synapse formation through the control of a not yet well-identified biological pathway(s).

In this study, we show that miR-218 is expressed in developing mesencephalic DAn and promotes the dopaminergic phenotype when expressed in embryonic stem cells (ESCs). Furthermore, miR-218 enhances dopaminergic differentiation, in primary cultured neurons and transdifferentiated fibroblasts, when combined with dopaminergic-related transcription factors generating functional DAn. We also show that miR-218 is involved in defining DAn excitability and neurotransmitter release capability through the regulation of an unpredicted synaptic related gene network, revealing its essential role in controlling the functional activity of DAn.

Materials and Methods

Lentivirus preparation and viral infection

Specific miRNA-encoding sequences were cloned into a PCR 2.1 TOPO TA cloning vector (Thermo) by using oligonucleotides flanked by the EcoRI recognition site. Subsequently, they were subcloned into Tet-O-FUW or Tet-O-FUW-Ires-GFP or Tet-O-FUW-Ires-Cherry lentiviral vectors (LVs), following the previously described method (De Gregorio et al., 2018).

Lentiviruses for mAscl1, mNurr1, mLmx1, and miRNAs were packaged in HEK293T cells as previously described (Caiazzo et al., 2011). Briefly HEK293T cells were cultured in DMEM, supplied with 10% FBS, 10 U/ml penicillin, and 10 µg/ml streptomycin (Pen/Strep), 2 mM L-glutamine, 1 mM sodium pyruvate, and 1× nonessential amino acids. A total of 7.5×10^6 HEK293T cells were seeded on 150 mm × 25 mm dishes, and the following day were transfected with 6.25 µg pRev, 9 µg pVSVG, 14.6 µg pMDL, and 32 µg of specific TET-O-FUW vector following the calcium phosphate transfection protocol. After 48 h, the supernatant was collected and ultracentrifuged at 68,000 × *g* in an SW28 rotor (Beckman Coulter; 67,840 × *g*) for 2 h at 20°C. The viral pellet was resuspended in PBS (Euroclone) and stored at −80°C. The infectivity of lentiviruses and the "maximum tolerated dose" were determined empirically through subsequent infections on HEK293T cells with increasing amounts of virus. Gene expression was tested by qPCR, while miRNA levels were measured by TaqMan assay. Infections were performed in combination with rtTA transactivator viruses, with or without doxycycline (DOX, 2 µg/ml, Clontech).

Ethics statement

All animal experiments have been approved by the Italian Ministry of Health (authorization 491/2017-PR) and conducted in strict accordance with national and European safety and ethical rules and regulations,

including to the Council Directive 2010/63/UE (published on September 22, 2010) regarding the protection of animals used for experimental and other scientific purposes, as well national legislations (Italian Legislative Decree 116/92 and Italian Legislative Decree 388/98). Every effort was made to minimize animal suffering and to reduce the number of animals used by following the principles of the 3Rs (replacement, reduction, refinement). The animals were bred in-house at the Institute of Genetics and Biophysics "Adriano Buzzati Traverso," Consiglio Nazionale delle Ricerche (Naples, Italy). All the procedures related to animal treatments were approved by Ethic Scientific Committee for Animal Experiments.

In this study, the following mouse lines were used and crossed: miR-218-1$^{-/-}$, miR-218-2$^{-/-}$, miR-218-2$^{fl/fl}$, Tg::TH$^{+/GFP}$ (Sawamoto et al., 2001), and the En1$^{Cre/+}$ (kindly provided by Prof. Antonio Simeone) (Kimmel et al., 2000). The mouse strains were maintained in an outbred C57Bl/6 background.

Generation of mouse mutant strains

The miR-218-1$^{-/-}$ and miR-218-2$^{-/-}$ (referred to as KO1 and KO2, respectively) were generated by using CRISPR/Cas9 dual-nickase mediated nonhomologous end joining following a previously published protocol (Ran et al., 2013). Briefly, two pairs of single guide RNA (sgRNA) targeting the miR-218-1 and the miR-218-2 genomic loci at both bottom and top strands were designed using the CRISPR double nickase design tool from the Feng Zang laboratory (https://www.zlab.bio/resources) and evaluated for their low off-target activity. Oligonucleotides containing the sgRNAs sequences and carrying two overhangs (5′ CACC on the forward and 5′AAAC on the reverse) were used for subcloning into BbsI digested pX335 vector.

Cas9n mRNA and sgRNA templates were amplified with T7 promoter sequence-conjugated primers and transcribed *in vitro* with mMESSAGE mMACHINE T7 Ultra Kit (Invitrogen) and MEGAshortscript T7 Kit (Invitrogen), respectively. The *in vitro* RNAs were injected into pronuclear stage fertilized mouse eggs, which were then transferred into the oviduct of pseudo-pregnant female mice (C57/Bl) (Ran et al., 2013). F1-mice carrying indels were mated with WT animals and subsequently Sanger-sequencing was performed on homozygotes DNA.

The conditional KO mouse model miR-218-2$^{fl/fl}$ (referred to as c-KO2) was generated through homologous recombination by the IGB Embryonic Stem Cells and Mouse modeling facility, following previously published methods (Puelles et al., 2003). The targeting molecule was generated from three intermediate PCR products that covered the Slit3 genomic region containing the miR-218-2 sequence (core) and two arms of homology upstream (long) and downstream (short). The PCR primers, as shown in Extended Data Figure 7-1*c*, contained specific restriction sites for ordered subcloning into pFrt3 as reported in Extended Data Figure 7-1. The BAC-A19 was used as template. The nucleotide sequence of the targeting molecule was verified by Sanger sequencing to exclude undesired mutations.

Homologous recombination events in electroporated E14tg4a2 ESCs were detected by PCR and confirmed by Southern blot using external and internal probes labeled with dCTP[α-^{32}P] as previously described (Acampora et al., 2009). PCR primers and probes are provided in Extended Data Figure 7-1*d*.

The ESCs containing the mutated allele were injected into the blastocyst and then implanted into foster pseudopregnant mice using standard procedures (Acampora et al., 1995). Germline transmission of the mutated allele was assessed in the F2 generation resulting from *chimera* × *WT* matings. The neomycin cassette was subsequently removed by mating miR-218-2$^{fl/+}$ mice with mice expressing the *Flp* recombinase. The screening for successful removal was performed by PCR (primers provided in Extended Data Fig. 7-1*d*).

Tissue collection

Mice brains and embryonal fibroblasts were dissected under sterile conditions in PBS, pH 7, without calcium and magnesium and in the presence of glucose (33 mM). Tissues were isolated under a stereomicroscope and processed for primary cultures, FACS, RNA extraction, or protein extraction.

For immunohistochemistry and RNA hybridization, E14.5 mice embryonic brains were rapidly dissected, fixed in 4% PFA, and subsequently embedded in wax dehydration with ethanol and treatment with xylene.

Mouse midbrain primary cultures (mE12.5-PCs) and high content imaging

Freshly prepared single-cell suspensions from mouse embryonic midbrain, referred to as mE12.5-PCs (mouse E12.5 primary cultures), were obtained following established protocols (Prochiantz et al., 1979; di Porzio et al., 1980; Pulcrano et al., 2022). In brief, the ventral midbrains from E12.5 embryos were carefully isolated and treated with 0.25% trypsin solution containing 0.01% pancreatic DNase for 5 min at 37°C. The tissues were then mechanically disrupted in complete culture medium supplemented with FBS, N2/B27 supplements, 0.5 mM L-glutamine, and penicillin/streptomycin. The resulting cell suspension was centrifuged at 100 × *g* for 5 min and plated at a density of 4×10^4 cells/cm^2 on poly-D-lysine-coated multiwells (15 μg/ml poly-D-lysine for 1 h at 37°C) in complete culture medium supplemented with fibroblast growth factor 8 (FGF8, 10 ng/ml) and sonic hedgehog (SHH, 50 ng/ml) to promote differentiation into DAn. For High Content Screening analysis, cells were plated on optical micro-well plates (96 or 384 MW) (Thermo).

After 3 d in culture (DIV3), LVs and DOX (2 μg/ml) were added to induce the expression of transgenes. At DIV6, medium was completely changed to remove SHH and FGF8. Cell samples were collected or fixed at DIV12.

For High Content Screening analysis, cells were fixed with 4% PFA and stained with antibodies TH and Nurr1 (using an anti-Flag antibody). The number of TH$^+$ and/or Nurr1$^+$ was automatically analyzed using the cell-based confocal microscope Opera Phenix (Perkim Elmer). At least 270 areas from four independent biological replicates were acquired. Data analysis, including the relative ratio of TH$^+$/Nurr1$^+$ cells, was performed using R software with one-way ANOVA and Benjamini-Hochberg's *post hoc* test, after standardizing values among all biological replicates.

Mouse ESCs (mESCs)

The ES-E14TG2a mESCs were cultured on gelatin-coated plate (0.1% in PBS) in Glasgow Minimal Essential Medium (Sigma) supplemented with 12% FCS, 1 mM sodium pyruvate, nonessential amino acids, 2 mM L-glutamine, 0.1 mM β-mercaptoethanol and LIF (300 U/ml Millipore), as described by Parmar and Li (2007).

To overexpress miR-218, the mESCs were plated at low density and infected with lentiviral particles after 1 d. Twelve hours after infection, the exogenous gene was activated by the administration of DOX, 4 μg/ml. Fluorescent cells were isolated with FACS ARIA (BD Falcon) 24-36 h after infection and plated in DOX-free medium.

To induce dopaminergic differentiation, the cells were plated on gelatin-coated plate in N2B27 medium, which is a mixture of half DMEM/F12 and half NBM supplemented with N2, retinol-free B27, 2 mM L-glutamine, and 0.1 mM β-mercaptoethanol. Four days after plating, the cells were passaged onto poly-L-lysine (15 µg/ml in PBS)/laminin (20 µg/ml in PBS) coated plates; and from day 5 to day 9 of differentiation, SHH (200 ng/ml) and FGF8 (100 ng/ml) were added to the medium while 2 μg/ml DOX was added from day 7 until the end of differentiation. The cells were cultured until day 14.

Induced DAn (iDAn) generation

To generate iDAn from mouse embryonic fibroblasts (MEFs), the method described by Caiazzo et al. (2011) was followed. In brief, MEFs were isolated from tg::TH$^{GFP/+}$ E14.5 mice embryos, which can be either WT or KO. The MEFs were plated at low density (25×10^3 cells/cm^2) in DMEM supplemented with 10% FBS, 2 mM L-glutamine, and Pen/Strep. After 24 h, the cells were infected with lentiviral particles carrying the transcription factors Ascl1, Nurr1, and Lmx1a in the presence or absence of miR-218-1 or miR-218-2 lentiviruses; and 24 h later, DOX (2 μg/ml, Sigma) was added to induce gene expression. At day 4 (DIV4) of the differentiation process, the medium was replaced with DMEM/F12, supplemented with B27, Pen/Strep, and DOX. The cells were cultured for 14-16 d, allowing them to differentiate into iDAn.

Flow cytometry
Separation and analysis of fluorescent cells were performed as previously described (Pulcrano et al., 2022). In brief, freshly dissected ventral midbrains of TH-GFP embryos or cells grown in monolayer were dissociated into single cells with 0.25% trypsin solution in 33 mM glucose/PBS with 0.01% pancreatic DNase. After dissociation, the trypsin was neutralized using PBS supplemented with 10% FBS. Cells were collected by short centrifugation, and the resulting pellet was resuspended in 500 μl PBS supplemented with 5%FBS and 0.01% DNase. The cell mixture was subjected to FACS using a BD FACSAria III instrument. The cells were sorted into GFP (and/or Cherry) positive and negative fractions. Cell suspensions intended for RNA extraction were stored in TRI-Reagent (Sigma) or RNA*later* (Ambion) for preserving RNA integrity. Alternatively, cell suspensions for subsequent amplification or cell culture experiments were stored in a suitable cell culture medium.

Cell suspensions from Pitx3-GFP and Lmx1a-GFP mice embryos were kindly provided by Prof. Marten P. Smidt and Prof. Thomas Perlmann, respectively.

RNA analysis (extraction, reverse transcription, and qPCR)
Total RNA was extracted from cells and tissues using either TRI-Reagent (Sigma) or mirVana miRNA Isolation Kit (Ambion) following the manufacturer's instructions. DNaseI (U/20 µl; Ambion) treatment to remove genomic DNA and spectrophotometry quantification preceded reverse transcription. For cDNA synthesis, 1 µg of RNA was used with iScript cDNA Synthesis Kit (Bio-Rad). qPCR was performed using iTaq Universal SYBR Green Supermix (Bio-Rad) on CFX-Opus (Bio-Rad) with a cDNA equivalent of 25 ng of total RNA per reaction in presence of 0.5 μM specific oligos.

The expression values for each gene were normalized to the hypoxanthine-guanine phosphoribosyl transferase (Hprt). The $2^{-\Delta Ct}$ method was used for normalization. The relative expression was calculated using the $2^{-\Delta\Delta Ct}$ formula (Livak and Schmittgen, 2001). For miR-218 precursors (pre-miR-218-1 and pre-miR-218-2), snRNA U6 and snoRNA-202 were used as normalizer (Antoniou et al., 2018). The qPCR analysis was conducted on at least triplicate samples for each experiment. Each sample was processed separately.

TaqMan miRNA assays
MiRNA expression analysis was performed by using TaqMan MicroRNA Assays (Applied Biosystems) accordingly to the manufacturer's instructions.

Briefly, the small-size RNA was isolated through the mirVana miRNA Isolation Kit (Ambion). Reverse transcription for mature miR-218 and miR-9, as well as for the reference snoRNA-202, was performed using a TaqMan MicroRNA Reverse Transcription Kit and TaqMan miRNA Assay specific for each miRNA according to the manufacturer's protocol (Applied Biosystems). qPCR was performed using primers and probe provided with the miRNA-specific TaqMan miRNA Assay along with the TaqMan Universal Master Mix II, no UNG (Applied Biosystems).

SDS-PAGE electrophoresis and immunoblotting
Western blot was conducted as previously described (Volpicelli et al., 2012, 2019). Briefly, tissues were harvested and lysed in RIPA buffer with protease inhibitors (Roche), followed by incubation on ice for 30 min. The lysate was clarified by centrifugation at 8000 × *g* for 10 min, and protein concentration was determined using spectrophotometry. Proteins (20 μg) and protein ladder (PageRuler Prestained, Thermo) were separated on 12% SDS polyacrylamide gel at 200 V for 80 min. Subsequently, the proteins were transferred to PVDF membranes (Immobilon-P, Millipore). The membranes were blocked in TBS-T 1× (0.1% Tween, 10 mM Tris-HCl, pH 7.5, 150 mM NaCl) and 5% nonfat milk for 1 h at room temperature and then probed with polyclonal anti-TH antibody (1:2000; AB152, Merk Millipore) and anti-mouse β-ACTIN antibody (Sigma-Aldrich, 1:10,000) for 2 h at room temperature. After three washes in TBS-T, the membranes were incubated with HRP-conjugated goat anti-rabbit IgG (GE Healthcare, 1:6000) or anti-mouse IgG antibodies (GE Healthcare, 1:6000). Protein bands were visualized by ChemiDoc (Bio-Rad) and enzyme-linked chemiluminescence (EMP012001, LiteAblot turbo, Euroclone). The relative protein levels were determined by densitometry using ImageQuant TL software and compared with the protein level of appropriate standard probed on the same membrane after stripping off the previously antibody. The intensity value of each band was obtained by subtracting the background of each area from the total intensity.

Immunocytochemistry
For immunostaining of cells grown in monolayer, we used the following protocol: cells were washed once with PBS, fixed in 4% PFA (Sigma) in PBS for 10 min, washed 3 times in PBS, and permeabilized 10 min in 0.3% Triton X-100/PBS (Sigma) (PBS-T). Cells were then blocked with 2% BSA (Sigma) and 5% of donkey serum (Biosera) in PBS-T for 45 min. Primary antibodies were incubated overnight at 4°C (anti-TH rabbit 1:500 Chemicon, catalog #AB152 and/or anti 3xFlag mouse Sigma, catalog #F3165). The next day, cells were washed in PBS-T and incubated 90 min with the fluorescence-labeled secondary antibody (1:200; AlexaFluor, Invitrogen) and counterstained with DAPI (1:1000; Invitrogen).

Immunohistochemistry and RNA hybridization on paraffin-embedded brain sections
Paraffin-embedded brains were sectioned in coronal slices with a thickness of 6-8 µm. Adjacent sections of paraffin-embedded brain section were processed either for RNA hybridization or for immunohistochemistry following the procedure described by Martinez-Morales et al. (2001) and Wilkinson (1992).

Sections were deparaffinized in BioClear and rehydrated with decreasing volumes of Ethanol (from 100% to 25%).

Immunohistochemistry. For antigen retrieval, sections were microwaved twice in 100 mM sodium citrate and 100 mM citric acid buffer, pH 6.0, boiling for 2 min 30 s: Sections were incubated in blocking solution (2% BSA, 5% NGS in PBS-T 0.1%) for 2 h. Primary antibody (anti-TH 1:500 rabbit AB152, Millipore; anti-ISL1 mouse 1:100, MABD131, Millipore; anti-PITX3 1:500, kindly provided by Prof. Marten Smidt) were diluted in blocking solution and incubated with the section for 2 h. After three washes in PBS-T, slices were incubated with a fluorescence-labeled secondary antibody (anti-mouse and/or anti-rabbit 1:200; AlexaFluor, Invitrogen) for 1 h. Sections were counterstained with DAPI (1:1000; Invitrogen) and mounted using 20% Mowiol.

Adult animals (p60) were perfusion-fixed with PFA 4% in PBS and sectioned using a vibratome. TH^+ neurons were visualized using a rabbit anti-TH (1:500; Millipore AB152) and an anti-rabbit-AlexaFluor-555 (1:200; Molecular probes). Optical sections were acquired with a Leica TCS SP5 confocal microscope.

ISH. Sections were treated with proteinase-K (10 µg/ml in 5 mM Tris-HCl, pH 7.4, 1 mM EDTA, 1 mM NaCl) at 37°C for 10 min and washed twice in PBS supplemented with 0.2% glycine. The slices were fixed in 4% PFA and washed again in PBS. Slices were treated with 0.1 M triethanolamine, pH 8.0, for 10 min, incubated in 0.1 M triethanolamine/0.25% acetic anhydride for 10 min followed by two washes in PBS.

Subsequently slices were probed with 100 µl of miR-218 diluted probe (miRCURY LNA Detection Probe, QIAGEN) following the manufacturer's instructions. Briefly, probe was diluted 1:1000 in hybridization buffer (5× SSC, 50% formamide, 5× Denhardt's solution, 500 µg/ml salmon sperm DNA, 250 µg/ml tRNA), denatured at 65°C for 5 min, and added to the sections for incubation at 20°C. After hybridization, washes were performed as follows: 5× SSC wash (5 min), 50% formamide/2× SSC (45°C, 35 min), 2× SSC (5 min), TBS-T (5 min).

Sections were blocked in 100 µl of 10% sheep serum/TBS-T for 30 min and then treated with 100 µl of anti-digoxigenin-AP (1:500 in blocking buffer; Merck) for 2-3 h at 4°C in humidified chamber.

After TBS-T wash, the sections were incubated in NBT/BCIP solution (Sigma) overnight until staining was completed. The sections were mounted with 20% Mowiol after two washes in TBS-T.

Microscopy (image quantification)
Images for ISH (bright field) and immunohistochemistry (fluorescence) were captured using a Leica DMI6000 inverted microscope at magnification 10× and 20×. To ensure consistency and comparability, images

were acquired with the same settings on the Leica Application Suite AF acquisition software. For cell counting, the number of positive cells was quantified using the ImageJ software. Specifically, a plug-in available on the software (rsb.info.nih.gov/ij/download/) was used for the quantification process. Quantification was performed on images obtained from a minimum of three independent experiments.

Confocal images, acquired with a Leica TCS SP5 confocal microscope, from control and $En1^{CRE}$ c-KO2 adult brain stained for TH, were quantified using the ImageJ environment. Quantification was performed on images obtained from a minimum of three independent experiments. The total number of TH^+ neurons per section were counted after application of a local threshold and watershed algorithm and defining the maximum and minimum particle size in a separate study with manually identified neurons. Neuronal density was defined as number of TH^+ per unit area (the ROI was manually defined by an experienced observed trained to identify the ventral midbrain). To confirm the results, we also measured the proportional area (percent of positive pixels over the ROI), which was independent from the identification of particles (neurons); positive pixels were identified by applying a local threshold algorithm.

Electrophysiology recordings

Midbrain and cortico-striatal slice preparation. WT, miR-218-$1^{-/-}$ (KO-1), miR-218-$2^{-/-}$ (cKO-2), and miR-218 double KO mice (c-dKO) aged P40-P60 were used for electrophysiological and amperometry recordings. The mice were deeply anesthetized using halothane inhalation and subsequently decapitated. The brain was quickly extracted from the skull and placed in chilled aCSF solution composed of the following (in mM): NaCl 126, $NaHCO_3$ 24, glucose 10, KCl 2.5, $CaCl_2$ 2.4, NaH_2PO_4 1.2, and $MgCl_2$ 1.2, saturated with 95% O_2–5% CO_2 gas mixture, pH 7.3. A tissue block containing either the midbrain or the cortex and striatum was glued to a plate and positioned within the chamber of a vibratome (Leica VT 1200 S) filled with chilled aCSF, saturated, and continuously gassed with a 95% O_2–5% CO_2 gas mixture. The horizontal slices with a thickness of 250 µm containing the SN pars compacta (SNpc) and the coronal cortico-striatal slices with a thickness of 300 µm, obtained with the vibratome, were transferred to a holding chamber containing aCSF at the temperature of 32°C, and allowed to recover for at least 1 h before usage (Guatteo et al., 2017; Federici et al., 2014).

Electrophysiological recordings in midbrain slices. A single brain slice was transferred in the recording chamber of an upright microscope (BX51WI; Olympus) and perfused continuously with aCSF at a rate of 2.5-3.0 ml/min The aCSF temperature was maintained at 33.0 ± 0.5°C. The SNpc dopamine neurons were identified using the following criteria (Krashia et al., 2017; Aversa et al., 2018; Martini et al., 2019): (1) their location in close proximity of the medial terminal nucleus of the accessory optic tract (MT); (2) the presence of eGFP when excited with UV light at 480 nm (emission filter, 510 nm) provided by a monochromator (Polychrome IV; Till Photonics) via a 40× water-immersion objective; the emitted light was detected by a CCD camera (Evolve; Photometrics); (3) the presence of a slow, regular pacemaker firing (0.5-8 Hz) in cell-attached configuration; (4) the presence of a hyperpolarization-activated (I_h) current in response to hyperpolarizing voltage commands (−60 to −120 mV, 20 mV increment) (Mercuri et al., 1995; Cucchiaroni et al., 2011; Guatteo et al., 2013), from $V_H = -60$ mV; and (5) the presence of eGFP when excited with UV light at 480 nm (emission filter, 510 nm) provided by a monochromator (Polychrome IV; Till Photonics) via a 40× water-immersion objective. The emitted light was detected by a CCD camera (Evolve; Photometrics). Recording pipettes were pulled using thin-wall capillaries (WPI) and filled with an intracellular solution containing the following (in mM): 125 K-gluconate, 10 KCl, 10 HEPES, 2 $MgCl_2$, 4 ATP-Mg_2, 0.3 GTP-Na_3, 0.75 EGTA, 0.1 $CaCl_2$, 10 phosphocreatine-Na_2. The solution had a pH of 7.2 and an osmolarity of ∼280 mOsm. Cell-attached recordings were initiated as soon as a seal resistance ≥1 GΩ was achieved, just before membrane rupture, with Axoscope software in voltage clamp ($V_H = -60$ mV; sampling 1 kHz). Membrane resistance (R_m) was measured by means of Clampex 9 Membrane Test protocol, within 2 min after membrane rupture, consisting of a 30-ms-long, − 5 mV step from $V_H = -60$ mV (33.3 Hz). A mean of 20 consecutive measurements was used to calculate final values. I_h current was elicited by 8 voltage steps (−50 to −120 mV, 10 mV increment, 2 s) from $V_H = -50$ mV. To analyze neuronal excitability, a current-clamp protocol consisting of 2 s current steps from 0 to 250 pA (10 pA increments) was delivered to SNpc DAn, while maintaining their membrane potential at $V_H = -60$ mV. The mean instantaneous frequency was calculated by averaging the frequency of the first two action potentials (APs) evoked at each stimulus intensity with a sampling rate of 20 kHz. Rheobase was defined as the first depolarizing current amplitude (pA) required to evoke an AP. The current underlying the AP after hyperpolarization (I_{AHP}) was elicited by a voltage command to 0 mV, from $V_H = -60$ mV, 100 ms duration. I_{AHP} peak (pA) and area (pA*ms) were measured with Clampfit software as maximal current amplitude and the area under the current trace, in a time window frame from the end of the voltage command up to 2 s time point.

Electrophysiological recordings from iDAn. A single coverslip with plated iDAn was placed in a recording chamber (0.6 ml) of an upright microscope (BX51WI; Olympus). The cells were continuously perfused (1 ml/min) with aCSF. The composition of extracellular aCSF and pipette solution used in the recordings was the same as that used for electrophysiological recordings in midbrain slices. The presence of eGFP and mCherry in iDAn was assessed using a 40× water-immersion objective. UV light at 480 nm (emission filter, 510 nm) and 495 nm (emission filter 590 nm) was provided by a monochromator (Polychrome IV; Till Photonics). The emitted light was detected by a CCD camera (Evolve; Photometrics). The voltage-dependent Na^+ and K^+ currents were elicited by depolarizing voltage steps ranging from −40 to 40 mV, in 5 mV increments of 300 ms, from a holding potential (V_H) of − 60 mV. INa^+ and IK^+ areas (nA*ms) were calculated by Clampfit software as the area under the current trace in a time window frame that included INa^+ or IK^+ at each voltage commend. Current-clamp recordings of APs were obtained from $V_H = -60$ mV in response to depolarizing current injections (15-105 pA, 10 pA increment, 300 ms). The data shown in Figures 4*l* and 6*n*, representing the number of evoked APs in WT iDAn, refer to the same experimental group, as they were obtained by the same reprogramming conditions (ANL).

Constant potential amperometry (CPA). Amperometric detection of dopamine (DA) release was performed as described by Nobili et al. (2017). A bipolar nickel/chromium-insulated stimulating electrode was used to deliver electrical pulses to the dopaminergic fibers innervating the dorsal striatum. A single rectangular electrical pulse delivered by a DS3 Stimulator (Digitimer) was applied to evoke the release of DA. Following a protocol of increasing stimulation intensity (40-1000 µA, 40-80 µs duration), a plateau of DA release was reached. The amount of DA release was detected as amperometric current by CPA, by means of carbon fiber electrode (active surface 30 µm in diameter and 100 µm long, WPI) gently positioned into the slice to a depth of 100-150 µm, in the close vicinity of the stimulating electrode and connected to a potentiostat (MicroC, WPI). The imposed voltage between the carbon fiber electrode and the silver/AgCl pellet was 0.6 V. The conversion of amperometric current into DA concentration was performed at the end of each experiment, by recording currents evoked by bath application of known DA concentrations ranging from 0.3 to 10 µM (Federici et al., 2014). The evoked amperometric current primarily represents extracellular DA overflow (Federici et al., 2014; Guatteo et al., 2017) as it is not affected by serotonin or norepinephrine transporter blockers (fluoxetine and reboxetine, respectively) (Federici et al., 2014), suggesting a negligible contribution of these neurotransmitters to the recorded signal.

Upon electrical stimulation, a rapid rise in amperometric current occurred, which typically decayed back to baseline within ∼1.5 s. The amperometric current peak amplitude was calculated as the difference between peak and baseline current level before stimulus application. The latency was determined as the interval between stimulus artifact and current peak, while half decay was calculated as the time between the current peak and time at which it recovered at 50% of maximal amplitude. The signals were digitized using a Digidata acquisition system (Digidata 1440A) coupled to a personal computer running the Clampex 10 software.

Data source

The microarray data related to epiblast-derived stem cells (epiSCs) differentiated toward the dopaminergic phenotype can be accessed through

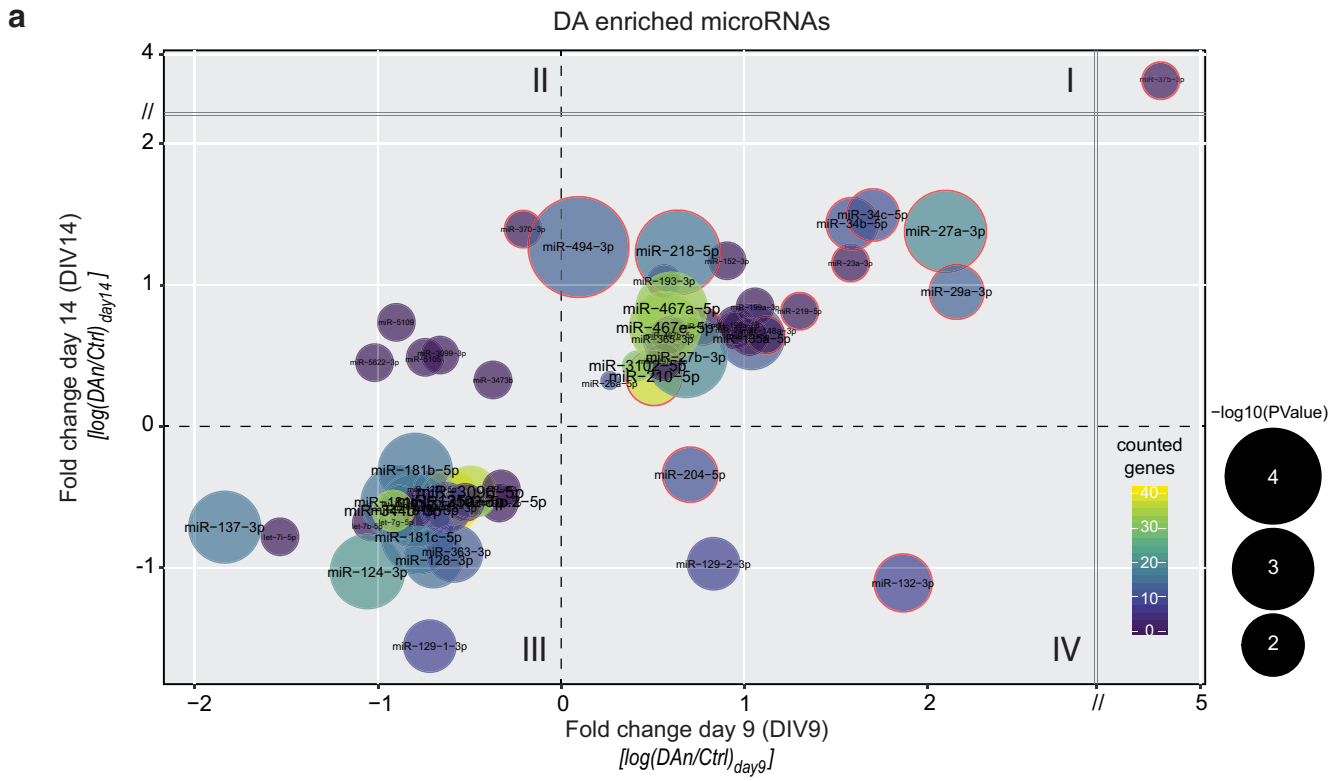

b

Always up

miRNA	FC-9	FC-14	DA genes	p-value
miR-375-3p	*4.81*	*3.83*	0	ns
miR-34c-5p	*1.70*	*1.50*	10	2.40E-02
miR-34b-5p	*1.59*	*1.43*	10	2.40E-02
miR-27a-3p	*2.10*	*1.38*	19	8.90E-04
miR-494-3p	*0.09*	*1.27*	13	4.00E-05
miR-218-5p	*0.64*	*1.23*	16	5.90E-04
miR-152-3p	*0.91*	*1.17*	0	ns
miR-23a-3p	*1.58*	*1.16*	0	ns
miR-193-3p	*0.56*	*1.03*	5	6.90E-02
miR-29a-3p	*2.16*	*0.95*	13	2.00E-02
miR-199a-3p	*1.06*	*0.85*	0	ns
miR-467a-5p	*0.60*	*0.84*	33	3.80E-03
miR-219-5p	*1.30*	*0.82*	0	ns
miR-199a-5p	*0.95*	*0.72*	0	ns

Always up

miRNA	FC-9	FC-14	DA genes	p-value
miR-210-3p	*0.78*	*0.71*	0	ns
miR-467e-5p	*0.57*	*0.70*	33	3.80E-03
miR-24-3p	*0.95*	*0.68*	0	ns
miR-148a-3p	*1.21*	*0.65*	0	ns
miR-467b-5p	*0.59*	*0.64*	0	ns
miR-21-5p	*1.03*	*0.64*	0	ns
miR-135a-5p	*1.04*	*0.63*	12	7.10E-03
miR-365-3p	*0.55*	*0.62*	6	5.50E-02
miR-27b-3p	*0.68*	*0.49*	19	8.90E-04
miR-297c-5p	*0.56*	*0.46*	0	ns
miR-3102-5p	*0.42*	*0.43*	30	7.90E-02
miR-210-5p	*0.51*	*0.34*	38	1.80E-02
miR-26a-5p	*0.27*	*0.32*	10	9.30E-02

Discordant

miRNA	FC-9	FC-14	DA genes	p-value
miR-370-3p	-0.21	1.40	0	ns
miR-132-3p	1.87	-1.11	8	1.50E-02
miR-204-5p	0.70	-0.34	10	1.90E-02
miR-129-2-3p	0.83	-0.97	8	2.40E-02
miR-3099-3p	-0.66	0.50	0	ns
miR-3473b	-0.37	0.33	0	ns
miR-5105	-0.74	0.49	0	ns
miR-5109	-0.90	0.74	0	ns
miR-5622-3p	-1.02	0.45	0	ns

Figure 1. Differentially expressed miRNAs in DAn differentiation. ***a***, miRNA expression during dopaminergic differentiation of epiSCs are represented as mean of the logarithmic ratio between DAn (SHH/FGF8) and Ctrl triplicate samples for both the differentiation time point DIV9 (*x* axis) and DIV14 (*y* axis). Only logFC values $\geq$ |0.5| were represented. For each miRNA, the bubble's color and size represent, respectively, the number of predicted target genes and the −Log(PValue) term enrichment in the KEGG pathway mmu04728:dopaminergic synapse. Targets were predicted using TargetScan 8.0 at default parameters. Red-circled miRNAs were selected for further analysis. ***b***, Fold changes of miRNAs upregulated during the whole differentiation process (always-UP) or with a fluctuating expression (Discordant).

the GEO database with the accession number GSE110270 as previously reported (De Gregorio et al., 2018). The RNA expression data in iDAn were retrieved from previously published paper (GEO: GSE27174) (Caiazzo et al., 2011).

Putative miRNA-mRNA interaction

For the identification of miRNA target genes with responsive elements within the 3′UTRs of protein coding genes (see Fig. 1), theTargetScan8.0 algorithm was used (version 8.0; https://www.targetscan.org/mmu_80/) (Agarwal et al., 2015).

To identify target genes for miR-218, miR-29a, miR-34b/c, and miR-204 (see Fig. 6; Extended Data Fig. 7-1), a combination of four different algorithms was used: TargetScan8.0 (version 8.0; https://www.targetscan.org/mmu_80/) (Agarwal et al., 2015); DIANA-microT-CDS (http://diana.imis.athena-innovation.gr/DianaTools/index.php) (Paraskevopoulou et al., 2013); miRDB (https://mirdb.org/) (Yuhao and Xiaowei, 2020); and PicTar (https://pictar.mdc-berlin.de/) (Krek et al., 2005). The default web-tools parameters were used for each algorithm, with the exception of DIANA-microT-CDS, where the threshold for the miTG-score was lowered to 0.5 instead of 0.7.

Gene ontology (GO) and gene interaction analysis

To perform GO for overrepresented cellular component and biological process terms, we used ShinyGO version 0.76 with default parameters (http://bioinformatics.sdstate.edu/go/) (Ge et al., 2020); whereas for the analysis of specific synaptic-related terms, we used SynGO (https://www.syngoportal.org/) (Koopmans et al., 2019).

To identify specific targets in the KEGG pathway *mmu04728: Dopaminergic synapse*, the list of genes in *mmu04728:Dopaminergic synapse* was downloaded from the KEGG database (https://www.genome.jp/kegg/) (Kanehisa et al., 2010) The list was then intersected with the list of TargetScan-predicted target genes for each miRNAs mentioned in Figure 1.

The targets network was established on the basis of protein–protein interactions and relations investigated by the STRING database version 11.5 (https://string-db.org/cgi/input?sessionId=boGAYG1amluN&input_page_show_search=on) (Szklarczyk et al., 2014).

Statistical analysis

The statistical analyses for the study were performed using GraphPad Prism (GraphPad Software) and OriginPro 2019 software. The specific tests used to assess the significance of differences between groups or conditions are described in the respective figure legends. The choice of statistical tests may vary depending on the experimental design and the type of data being analyzed.

Results

miR-218 is upregulated during DAn differentiation

To identify miRNAs involved in DAn development and differentiation, we have previously performed an miRNA-mRNA paired microarray analysis from epiSCs, differentiated toward the dopaminergic phenotype at different maturation stages corresponding to early (day 9, DIV9) and late (day 14, DIV14) *in vitro* differentiation (De Gregorio et al., 2018). A total of 169 differentially expressed miRNAs were identified by comparing epiSCs differentiated into DAn with epiSCs differentiated into nondopaminergic neuronal phenotype (Ctrl). Of these 169 candidates, 67 miRNAs showed differential expression at both DIV9 and DIV14 with a fold change $> |0.5|$ in at least one of the two temporal points.

The miRNAs were grouped into three main clusters based on their expression patterns during the differentiation process. This was achieved by plotting the relative expression of each miRNA at the DIV9 (x axis) and DIV14 (y axis) as fold change ($\log_2$DAn/Ctrl). The clustering analysis revealed miRNAs that were consistently upregulated during the entire differentiation protocol (always-UP, in the first quadrant, Fig. 1*a*,*b*), miRNAs downregulated at both DIV9 e DIV14 (always-DOWN, third quadrant), and miRNAs with discordant expression profile at DIV9 and DIV14 (second and fourth quadrants, Fig. 1*a*,*b*).

To assess the correlation of each miRNA with genes involved in the development and functioning of DAn, the enrichment of target genes in the KEGG pathway mmu04728, dopaminergic synapse, was calculated for each miRNA's predicted target gene list using Targetscan 7.2. The significance of the enrichment was represented as Log(PValue), with different bubble sizes, whereas the color gradient, from purple to yellow, was used to represent the number of hits. miRNAs with no targets in the dopaminergic-related pathway were represented as small-size purple bubbles.

Since our focus was on miRNAs involved in the regulation of dopaminergic differentiation and function, we considered the miRNAs that showed upregulation during the differentiation process (in the first quadrant) as the most interesting candidates. For further analysis, we selected the miRNAs that exhibited the highest upregulation at both DIV9 and DIV14. Specifically, we chose miRNAs with a fold change ($\log_2$DAn/Ctrl) >1.2 in at least one time point (miRNAs underlined in Fig. 1*b*). These correspond to *miR-148a, miR-23a*, *miR-27a, miR-29a, miR-218*, *miR-219*, *miR-34b, miR-34c*, *miR-375-5p, miR-494*, and *miR-370*. We also included *miR-210* for its high number of potential target genes within the *DAsynapse*, KEGG pathway and two discordant miRNAs, *miR-132* and *miR-204*, whose expression increases only in early phases of differentiation, reminding of a potential role in the early phases of dopaminergic commitment as recently indicated by Pulcrano et al. (2022).

miR-218 promotes dopaminergic differentiation of mesencephalic primary neurons

To investigate the impact of the selected 14 miRNAs on dopaminergic differentiation, the genomic DNA sequences encompassing each miRNA were cloned into a DOX-inducible LV. Embryonic (E12.5) midbrain primary neurons were cultured in microwell plates and the dopaminergic differentiation was initiated by adding SHH and FGF8 for 6 d (Fig. 2*a*). On the third day of *in vitro* differentiation (DIV3), cells were infected with LV expressing the pro-dopaminergic transcription factor Nurr1 (cloned as 3xFlag-Nurr1, hereafter referred to as Nurr1) in combination with the desired miRNA-expressing LVs. To this purpose, we generated 12 LVs expressing each miRNA precursor (Fig. 2*b*). The miRNAs located in the same genomic region were cloned in a single construct, resulting in three constructs: *miR-34b/c* (*miR-34b* and *miR-34c)*; *miR-132* (containing also *miR-212*); and *miR-27a* (containing *miR-23a*, *miR-24-2* and *miR-3074-2*).

The cells were then cultured for a total of 12 d (DIV12). At the end of the differentiation protocol, the cells were fixed and stained for the dopaminergic marker TH and the flagged-NURR1 to identify DAn (TH^+) and infected cells ($NURR1^+$) (Fig. 2*c*). The fluorescent cells were automatically counted using the Opera High Content system. Data from five independent experiments were normalized, standardized, and expressed as the relative ratio between $TH^+/NURR1^+$ cells (Fig. 2*d*). $NURR1^+$ infected cells were used as a basal condition since uninfected cells, and cells overexpressing only the miRNAs were unable to induce TH (for a representative image of the reprogramming efficiency of miR-218-1 alone and in combination with Nurr1, see Fig. 2*e*; Fig. 2*f*). As a positive control, we used the combination of LMX1A with NURR1, as previous studies have shown that the coexpression of these two transcription factors enhances the generation of DAn *in vitro* (Caiazzo et al., 2011) (Fig. 2*c*,*d*). DAPI staining shows that a similar amount of cells was analyzed for each condition (Fig. 2*g*).

Each miRNA was tested in combination with NURR1 to evaluate its ability to promote TH expression. Among the tested miRNAs, only four were able to increase the number of TH^+ cells. These were miR-34b/c, miR-148a, miR-210 (with a nonsignificant trend), and miR-218-1 which appeared to be the most efficient in promoting dopaminergic differentiation with a significant twofold increase of TH^+ cells compared with Nurr1 alone (Fig. 2*d*). While we have shown, in previous studies, that miR-34b/c and the miR-148a promote dopaminergic differentiation through the regulation of the Wnt pathway (De Gregorio et al., 2018), the connection between miR-218 and DAn has only recently been established (Cuesta et al., 2018).

Dopaminergic differentiation of mESC and iDAn in the presence of miR-218

To understand the role of miR-218 in promoting dopaminergic differentiation, we expressed miR-218 in differentiating mESCs as they are known to be more responsive to dopaminergic differentiation stimuli if compared with already committed primary culture neurons (Ying et al., 2003). To this purpose, the mESCs were infected with DOX-inducible LVs expressing the pre-miR-218-1 (referred to as pre-miR-218) upstream of an Ires-GFP, while an inducible lenti-GFP was used as control. This approach allowed for the correct processing of the mature miRNAs and simultaneous visualization of infected cells (De Gregorio et al., 2018). The infected mESCs were treated with DOX for 1 d and GFP-expressing cells were purified by FACS. The GFP^+ mESCs were kept in the absence of DOX and then differentiated toward the dopaminergic phenotype in the presence or absence of DOX for 14 d (scheme in Fig. 3*a*). At the end of the differentiation protocol, the expression of miR-218 was evaluated by TaqMan-qPCR, resulting 30 times higher in DOX-treated cells compared with control cells (1 ± 0.1 vs 0.03 ± 0.007) (Fig. 3*b*). The ability

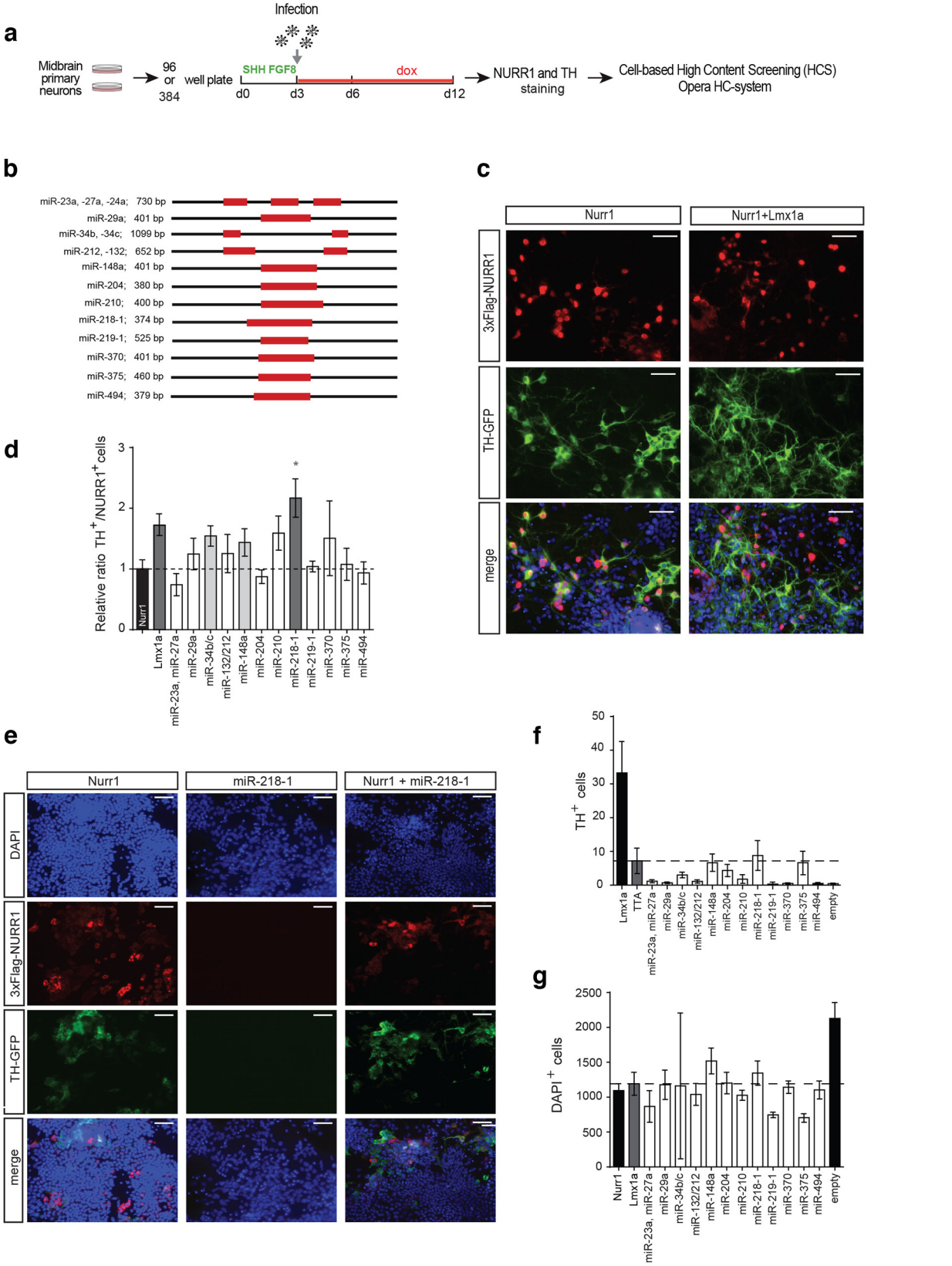

Figure 2. miR-218 upregulation positively affects dopaminergic differentiation. ***a***, Schematic representation of the experimental procedure adopted for cell-based High Content Screening. ***b***, Representation of the genomic sequences encompassing miRNAs genomic loci cloned into the TET-O-FUW plasmid for the production of inducible lentiviral particles (LVs) used to overexpress miRNAs. ***c***, Representative images of E12.5 midbrain primary cultures infected with LVs for Nurr1 alone or in combination with Lmx1a. Immunostaining was performed against 3xFlag-NURR1 (red) and Th (green), nuclei were stained with DAPI (blue). Images were acquired at 20× magnification. Scale bar, 50 μm. ***d***, Relative ratio of $TH^+/NURR1^+$ cells following lentiviral infection with 3xFlag-Nurr1 alone or in combination with LVs for different miRNAs. Cells infected with Nurr1 alone were used as basal control (=1). Data are mean ± SEM. $n = 270 \pm 80$ acquired fields from at least 5 independent experiments. *$p \leq 0.05$ (one-way ANOVA + Benjamini-Hochberg's *post hoc* test). ***e***, Representative images of E12.5 midbrain primary cultures (mE12.5-PCs) overexpressing

of miR-218 to promote dopaminergic differentiation was assessed by qPCR for the expression of specific dopaminergic markers as well as by immunostaining against TH. The mRNA levels of *Th*, *Pitx3*, *Nurr1*, and *Lmx1a*, which are markers of dopaminergic differentiation, were upregulated with a significant increase at day 12 and day 14 (Fig. 3*c*). Similarly, low-magnification images of mESC colonies differentiated toward the dopaminergic phenotype in the presence or absence of miR-218 showed a consistent increase in TH^+ colonies (Fig. 3*d*).

The role of miR-218 in promoting dopaminergic differentiation was further investigated during the direct *trans*-differentiation of MEFs into iDAn. *Trans*-differentiation of MEF into iDAn has been extensively studied as potential source of functional neurons for cell replacement therapy in Parkinson's disease patients. To this purpose, miR-218 was added to the *trans*-differentiation cocktail of transcription factors Ascl1, Nurr1, and Lmx1a (hereafter referred to as ANL) (Caiazzo et al., 2011).

To visualize cells expressing miR-218-1or miR-218-2, their precursors were cloned into a DOX-inducible lentivirus vector upstream of an Ires-Cherry sequence. MEFs derived from transgenic mice expressing the GFP under the control of *Th* promoter (TH-GFP) (Sawamoto et al., 2001) were infected at *in vitro* day 1 with the ANL lentiviruses cocktail in combination with miR-218-1 or miR-218-2 (Caiazzo et al., 2011; De Gregorio et al., 2018) and differentiated for 2 weeks (Fig. 4*a*). As revealed by qPCR, the expression of miR-218 was upregulated in both cases, with a 10-fold and fourfold increase for miR-218-1 and miR-218-2, respectively, compared with U6 snRNA or sno202 RNA (Fig. 4*b*).

The ability of miR-218 in promoting iDAn differentiation was confirmed by the upregulation of DA markers, such as *Th* and *Vmat2*, indicating a more pronounced dopaminergic phenotype, although no significant changes were observed for *Pitx3* and *Dat* (Fig. 4*c*). The increases of iDAn were assessed by manually counting of TH-GFP^+ cells in at least five different fields for each well in four independent *trans*-differentiation experiments ($n > 20$). The counting was performed by normalizing for the area analyzed (for representative images, see Fig. 4*d*; Fig. 4*e*). A similar result was obtained using flow cytometry to determine the percentages of TH-GFP^+ cells within the miR-218-1(−2) $Cherry^+$ and $Cherry^-$ cell populations (Fig. 4*f*,*g*). The addition of lentivirus for miR-218-1(−2)-Ires-Cherry to the reprogramming cocktail increased the number of iDAn by up to threefold in each well (Fig. 4*h*).

The enhanced dopaminergic phenotype observed in iDAn expressing miR-218 in combination with ANL was accompanied by a functional increase in their ability to fire APs, compared with iDAn generated only with ANL (TH^+ miR-218-$Cherry^+$ vs TH^+; Fig. 4*j*–*l*). Although the *I*–*V* relationships of the ionic currents underlying APs (voltage-gated Na^+ and K^+ currents) were similar between TH^+ miR-218-$Cherry^+$ and TH^+ iDAn (Fig. 4*j*, *k*), the number of APs generated in response to depolarizing current injections (15-105 pA, Fig. 4*l*) was higher in TH^+ miR-218-$Cherry^+$ iDAn, suggesting a significant change in cell intrinsic excitability associated with dopaminergic differentiation.

←

by LVs Nurr1 and/or miR-218-1 and differentiated for 12 d. Cells were stained for 3xFlag (exogenous NURR1, red), TH (green), and DAPI (blu). Images were acquired at 20× magnification of a Leica DMI600 microscope. Scale bar, 50 μm. ***f***, ***g***, Automatic counts of TH^+ (***f***) and total (***g***) cells from mE12.5-PCs overexpressing single miRNAs or Nurr1 (3x-Flag). Total cells were identified with the nuclear dye (DAPI), while TH^+ cells were stained for TH as control cells infected with the only rtTA were used. Dashed lines indicate the mean for Ctrl values.

miR-218 is expressed, *in vivo*, in mesencephalic DAn

Our data point to a role of miR-218 in the *in vitro* process of DAn differentiation. To understand the contribution of miR-218 to DA neuron development *in vivo*, we evaluated the expression of miR-218 during the embryonic development of the mouse midbrain. To this purpose, we purified GFP^+ neurons from the TH-GFP mouse line, where the GFP was located downstream of the *Th* promoter and from the *Pitx3*-GFP and *Lmx1a*-GFP mouse line where the mDA neurons were exclusively labeled by the knock-In GFP reporter (Zhao et al., 2004 and Deng et al., 2011, respectively). Interestingly, miR-218 was found to be enriched in the GFP^+ neurons sorted from these three lines compared with GFP^- cells. In all cases, the expression of miR-218 was at its highest between E12.5 and E14.5 (Fig. 5*a*). In contrast, miR-9, a neuronal miRNA (Alwin Prem Anand et al., 2020), did not appear significantly enriched in GFP^+ cells (Fig. 5*b*).

Furthermore, we evaluated the expression of miR-218 in DAn of E14 midbrain coronal sections using immunofluorescence, for midbrain markers, and miRNA ISH. We observed that miR-218 was detected in cell expressing *Islet1*, a transcription factor associated with oculomotor neurons, but was also expressed, albeit at lower levels, within the dopaminergic precursor domain characterized by the expression of TH and PITX3 (Fig. 5*c* and magnification).

The role of miR-218 in dopaminergic differentiation was further demonstrated by the upregulation of endogenous miR-218 during the dopaminergic *in vitro* differentiation of different cell types, including epiSCs, midbrain primary cultures (mE12.5-PCs), and MEFs (iDAn) (Fig. 5*d*). These findings indicate that the expression of miR-218 is triggered during dopaminergic differentiation and suggest its potential role in this process.

Deletion of miR-218 alters iDAn excitability

To investigate the role of miR-218 in DAn function, we generated constitutive KO mice for both miR-218-1 and miR-218-2 by using the CRISPR/Cas9 approach (hereafter referred to as KO1 and KO2, respectively). Two pairs of gRNA were used to delete a 136 bp, including the entire *pre-miR218-1* sequence (110 bp) and a 30 bp at the 5′ end of *pre-miR-218-2*, resulting in the deletion of 14 of 21 nucleotides of the mature miR-218-5p (Fig. 6*a*,*b*). The null alleles exhibited Mendelian transmission without notable phenotypic differences among littermates until birth, at which point single miR-218-$2^{-/-}$ pups or double miR-218-$1^{-/-;}$ miR-218-$2^{-/-}$ pups died (hereafter referred to as dKO; Fig. 6*c*, Table 1; Movie 1) consistently with previous observations (Amin et al., 2015, 2021).

The absence of miR-218 expression was confirmed by TaqMan analysis in the midbrains of single and double KO (dKO) embryos at E14.5, when miR-218 expression is highest. KO1 embryos showed a 55% reduction of miR-218 expression, while KO2 embryos exhibited a 30% reduction. As expected, no detectable expression of miR-218 was observed in dKO embryos (Fig. 6*d*). Furthermore, the deletion of miR-218-1 and miR-218-2 did not significantly affect the expression of the *Slit2* and *Slit3* host genes (Fig. 6*e*).

To assess the impact of miR-218 deletion on DAn development, we examined the expression of specific dopaminergic markers in the midbrain. We observed no changes in *Th* mRNA expression (Fig. 6*f*) nor a reduction of TH^+ cells in E14.5 midbrains, as determined by FACS analysis (Fig. 6*g*) and immunofluorescence staining on midbrain coronal sections (Fig. 6*h*,*i*). Similarly, the quantification of $PITX3^+$ (Fig. 6*h*,*j*) or ISLET-1^+

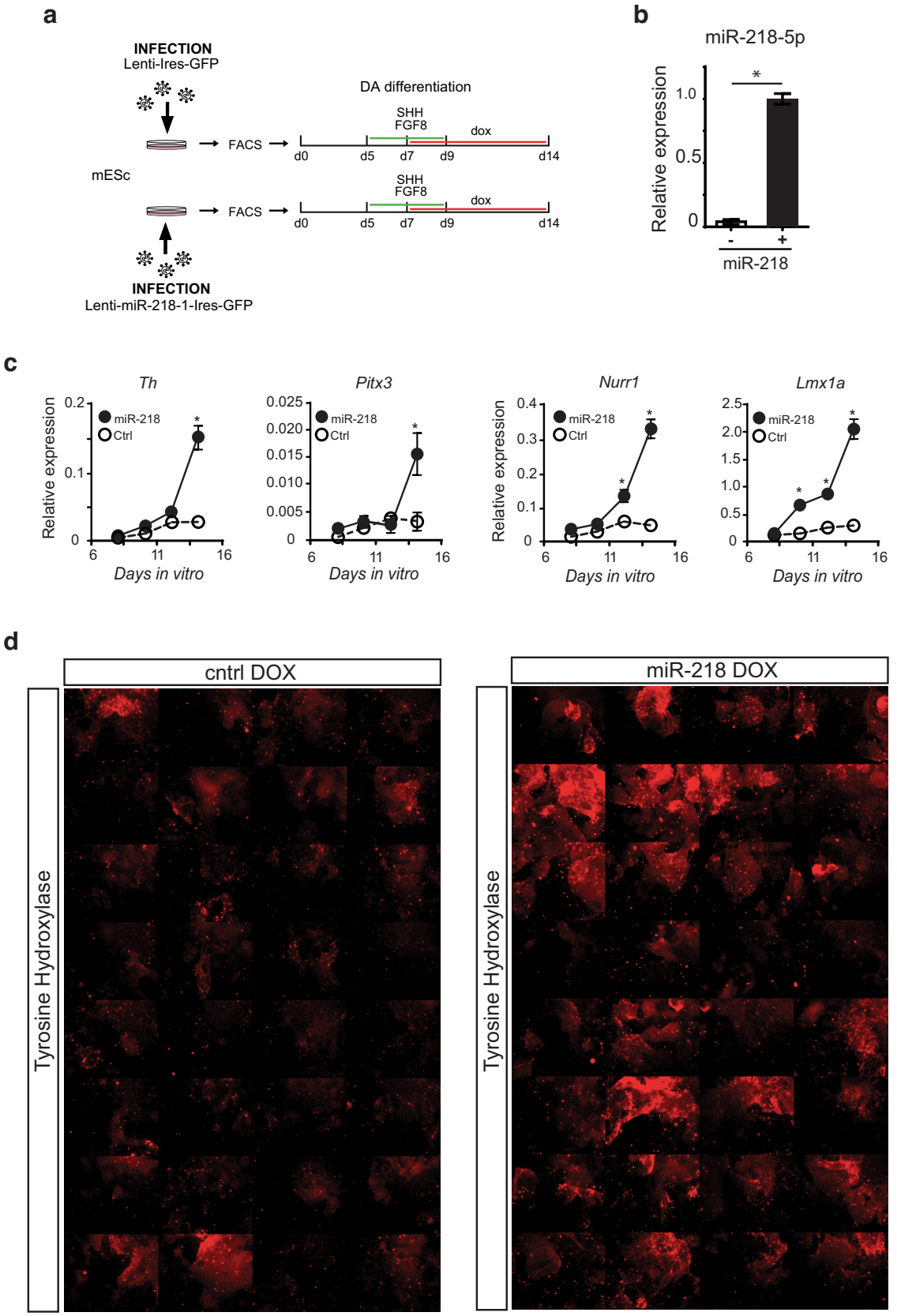

Figure 3. miR-218 promotes mESC differentiation into DAn. ***a***, Schematic representation of the experimental procedure of mESCs infected with a DOX-inducible LV expressing miR-218-1 upstream of an Ires-GFP sequence (or Ires-GFP empty vector), FACS-purified and amplified, before DA differentiation. ***b***, TaqMan assay for miR-218 from FACS-purified mESCs infected with LVs for miR-218-Ires-GFP or empty Ires-GFP. Data were normalized to the average of the reference sno-202. Data are mean ± SEM of $2^{-\Delta Ct}$ values. *$p < 0.05$, $n = 3$ (Student's t test). ***c***, The expression of dopaminergic genes (Th, Pitx3, Nurr1, and Lmx1a) was analyzed by qPCR, during the differentiation protocol in the presence or absence of DOX. Data are mean ± SEM from three independent experiments. *$p < 0.01$ (Student's t test). ***d***, Immunostaining for Th in FACS-sorted, amplified, and differentiated in mESCs infected with LVs for miR-218-Ires-GFP or an empty Ires-GFP, as control, in presence of DOX. A panel of 32 low-magnification images (5×) for each condition is shown.

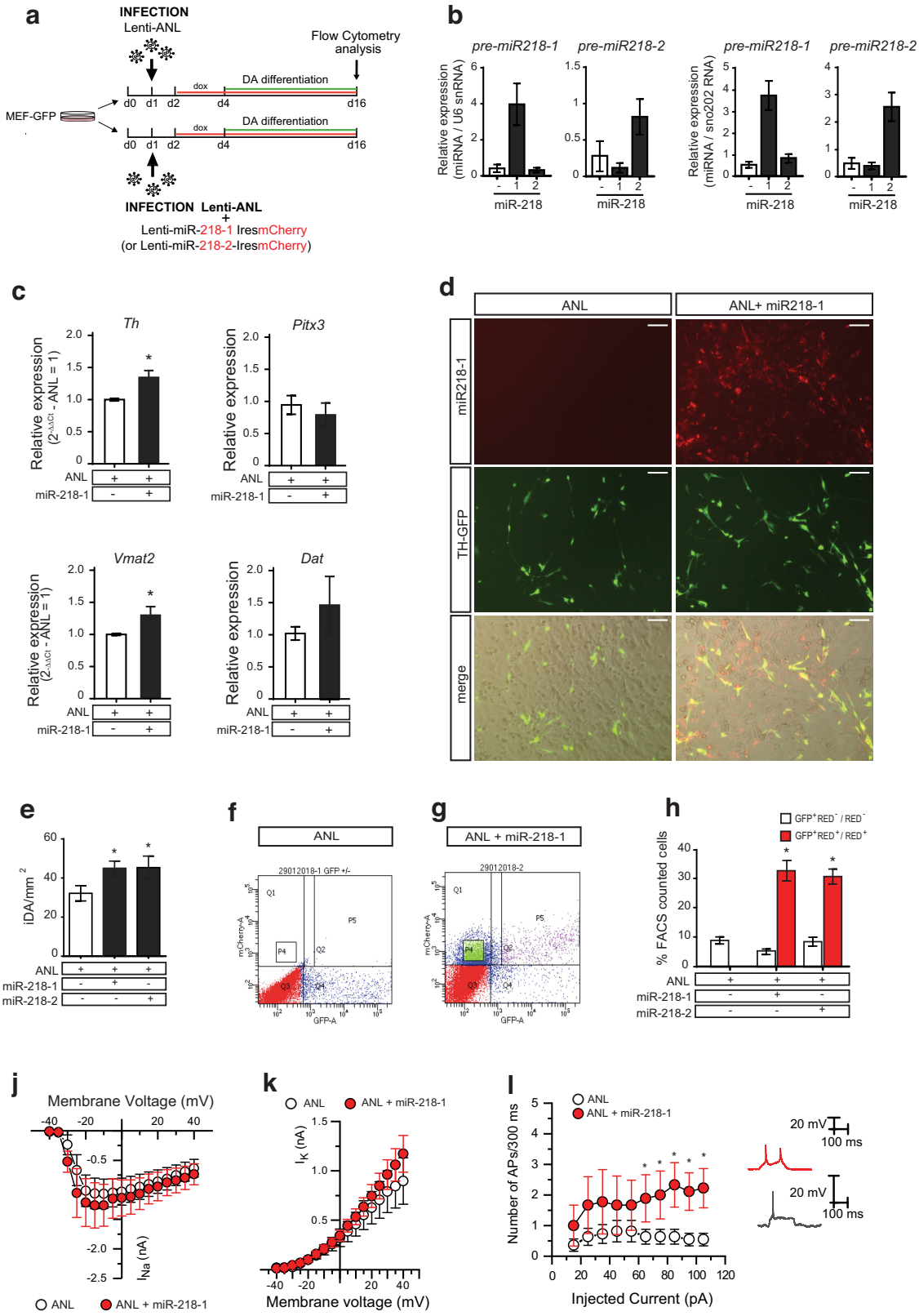

Figure 4. The expression of miR-218 in iDAn improves dopaminergic differentiation. ***a***, Procedural scheme for *trans*-differentiation of MEFs into iDAn after miR-218-1 or miR-218-2 overexpression. MEFs from E14.5 tgTH$^{GFP/+}$ mouse embryos were infected with the transcription factors Ascl1, Nurr1, and Lmx1a (ANL) alone or in combination with the miR-218-1 (or miR-218-2) cloned upstream Ires-mCherry sequence and differentiated for 2 weeks. ***b***, qPCR for pre-miR-218-1 and pre-miR-218-2 on iDAn overexpressing the two different isoforms. U6 snRNA and sno-202 RNA were used for normalization. Data are mean ± SEM of $2^{-\Delta Ct}$ values. *$p < 0.05$, $n = 4$; Kruskal–Wallis test plus Dunn's multiple comparison correction. ***c***, The expression of Th, Pitx3, Vmat2, and Dat was analyzed by qPCR in iDAn overexpressing miR-218-1. Data are mean ± SEM from three independent experiments. *$p < 0.05$ (Student's *t* test). ***d***, iDAn *trans*-differentiation efficiency is shown in the representative pictures obtained through the overexpression of Ascl1, Nurr1, and Lmx1a (herein ANL) in combination with the miR-218-1-Ires-Cherry into MEFs isolated from tgTH$^{GFP/+}$ mice. Images were acquired with DMI6000 at 20× magnification. Scale bar, 100 μm. ***e***, The number of iDAn was evaluated by counting Th-GFP$^+$ or Th-GFP$^+$/mCherry$^+$ cells. Manual counting was performed at least on five different fields for each well in four independent *trans*-differentiation experiments ($n > 20$) and normalizing for the analyzed

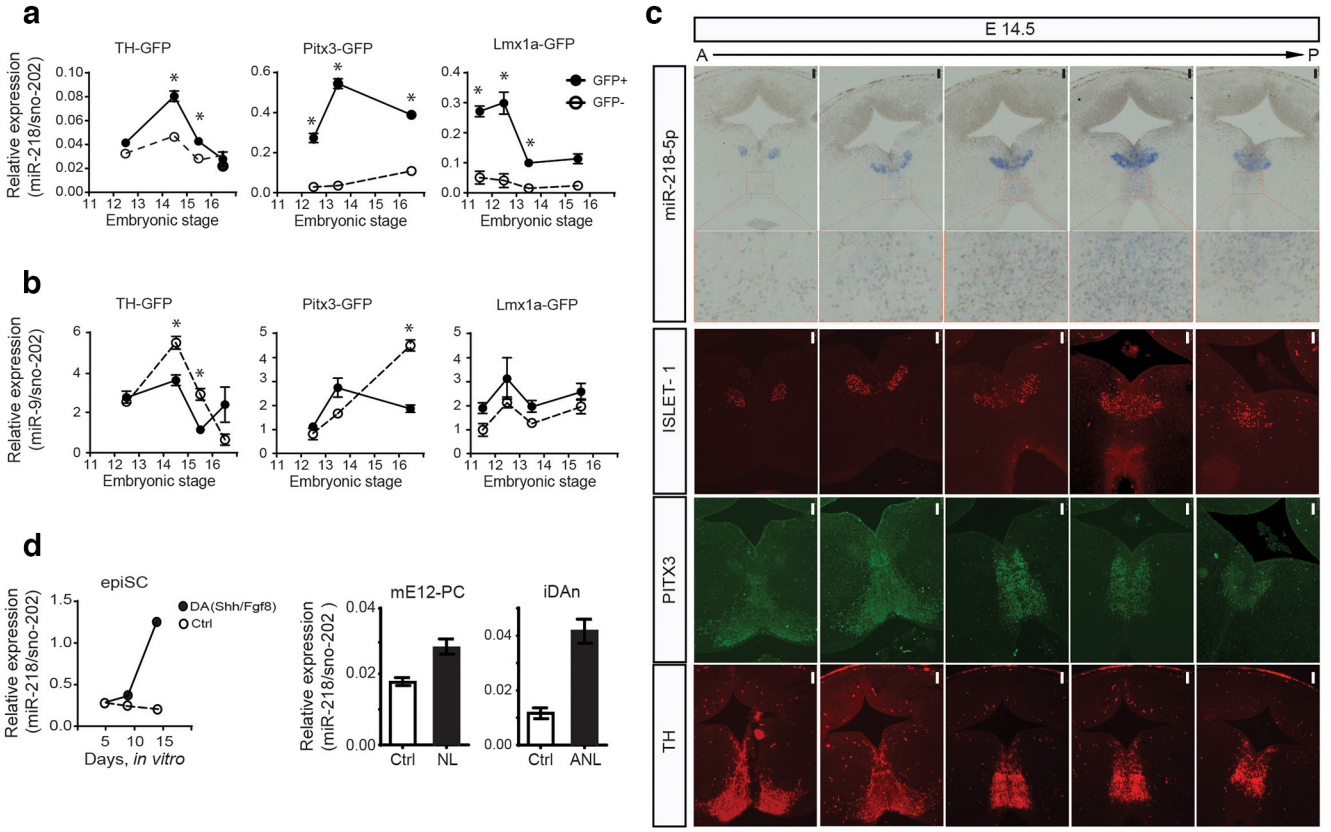

Figure 5. miR-218 is expressed in mesencephalic DA nuclei during mice development. ***a***, ***b***, TaqMan assay for the expression of miR-218 (***a***) and miR-9 (***b***) in FACS-purified GFP^+ and GFP^- cells from Th-GFP, Pitx3-GFP, and Lmx1a-GFP reporter mouse embryos at different developmental stages. Data are normalized to the average of the reference sno-202 and represent the mean ± SEM of $2^{-\Delta Ct}$ values from three independent experiments. *$p < 0.05$ of GFP^+ with respect to GFP^- (two-way ANOVA followed by Sidak). ***c***, ISH for miR-218 and IHC for Islet1, Pitx3, and Th (markers, respectively, of oculomotor and dopaminergic midbrain nuclei) in coronal section of brains from E14.5 mouse embryos. Consecutive sections were stained for the different markers (different lanes) while disposed with an anteroposterior order (on the same lane). Magnification for miR-218 ISH on DA nuclei is shown in the second lane. Scale bars: ISH, 75 μm; IF, 100 μm. Digital magnification is 4.2×. ***d***, TaqMan assay for the expression of miR-218 in DAn differentiated from epiSCs (left); E12 neuronal progenitor cells (mE12-PCs) expressing the pro-dopaminergic transcription factors Nurr1 and Lmx1a (NL) (middle); and iDA cells transdifferentiated with the reprogramming cocktail ANL (Asl1, Nurr1, Lmx1a) (right). Data are normalized to the average of the reference sno-202 and represent the mean ± SEM of $2^{-\Delta Ct}$ values from three independent experiments. *$p < 0.05$ of GFP^+ with respect to GFP^- (two-way ANOVA followed by Sidak).

(Fig. 6*h*,*k*) cells in E14 coronal sections revealed no significant differences. These findings suggest that embryonal loss of miR-218 has minimal impact on the differentiation of DAn and non-DAn in the midbrain.

We then investigated the consequences of miR-218 complete deletion on neuronal excitability. To this purpose, we generated iDAn from E14 miR-218 dKO fibroblasts and performed electrophysiological analysis by means of whole-cell patch-clamp technique. We found that the voltage-gated potassium (I_{K^+}, Fig. 6*l*) and sodium currents (I_{Na^+}, Fig. 6*m*) were increased in dKO iDAn compared with controls, as revealed by I_{K^+} and I_{Na^+} current area analysis. Also, the number of evoked APs in response to increasing intensity stimuli increased significantly (Fig. 6*n*) in dKO iDAn. These data indicate that miR-218 contributes to the regulation of DAn excitability as its deletion from the genome significantly perturbs I_{K^+}, I_{Na^+}, and AP firing.

Midbrain specific deletion of miR-218 affects the nigrostriatal circuitry

To overcome the lethality associated with miR-218-$2^{-/-}$ and gain further insight into its role in dopaminergic development and function, we generated a conditional KO mouse line for miR-218-2. This was achieved by inserting two loxP sites located 487 bp upstream and 416 bp downstream the pre-miR-218-2 locus, using homologous recombination (miR-218-$2^{fl/fl}$; Fig. 7*a*; Extended Data Fig. 7-1*a*,*b*). The conditional allele was then crossed with the $En1^{Cre}$ mutant mice which carry a *Cre* recombinase (Cre) "knock-in" allele in the *Engrailed-1* locus enabling the

←

surface. Data are mean ± SEM. ANL: 27.09 ± 3.82/mm^2 versus ANL218-1: 46.63 ± 3.7/mm^2 versus ANL218-2: 47.47 ± 6.05/mm^2; respectively, $p = 0.0055$ and $p = 0.0298$ with one-way ANOVA nonparametric Kruskal–Wallis test and Dunn's multiple comparison correction. $n \geq 3$ biological x2 technical. ***f***, ***g***, Ctrl (ANL) and miR-218-1-Ires-mCherry (ANL+miR218-1) overexpressing iDAn analyzed by FACS. ***h***, The number of total $TH\text{-}GFP^+$ cells was normalized with $Cherry^+$ miR-218-1 (miR-218-2) cells. Data are mean ± SEM. ANL: 9.11 ± 1.3 versus ANL218-1: 32.99 ± 3.51, $p = 0.0049$; ANL versus ANL218-2: 31.02 ± 2.57, $p = 0.0099$; one-way ANOVA nonparametric test Kruskal–Wallis test and Dunn's multiple comparison correction. $n \geq 3$ biological x2 technical. ***j-l***, Functional characterization of iDAn obtained by *trans*-differentiation of MEFs with and without miR-218-1. iDAn were identified as $TH\text{-}GFP^+$ or as double positive: $TH\text{-}GFP^+$, miR-218-$mCherry^+$, revealed that voltage-dependent Na^+ (***i***) and K^+ (***j***) currents displayed nearly overlapping current to voltage relationships in the two groups Data are mean ± SEM. Two-way repeated-measures ANOVA, Bonferroni test (not significant). Nevertheless, iDAn overexpressing miR-218-1 in combination with ANL produce a higher number of APs (***k***) in response to depolarizing current injections (15-105 pA, 10 pA increment, 300 ms) compared with iDAn generated only with ANL ($TH\text{-}GFP^+$) Data are mean ± SEM. 65 pA and 75 pA, $p < 0.05$; 85-105 pA, $p < 0.01$; two-way repeated-measures ANOVA followed by Tukey test. Representative traces were reported in the quadrant.

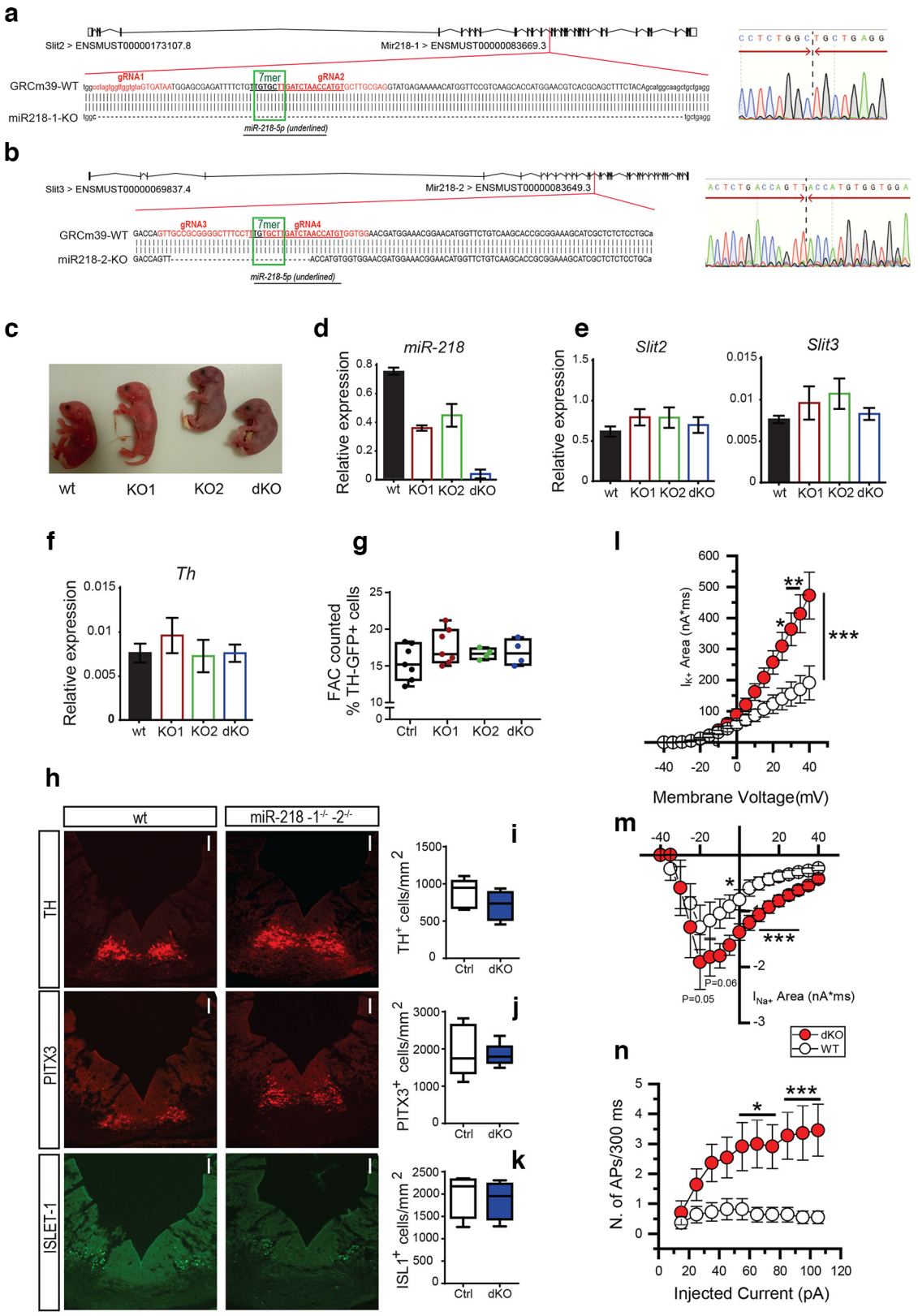

Figure 6. Constitutive deletion of the miR-218. ***a***, ***b***, CRISPR-cas9-mediated deletion of miR-218-1 and miR-218-2 by using two gRNAs for each targeted locus. The chromosomic regions containing Slit2 and Slit3 and the location of miR-218-1 and miR-218-2 within these genes are reported in ***a*** and ***b***, respectively. Uppercase letters represent the pre-miRNA sequences. Red represents gRNAs. The sequences of mature miRNAs are underlined. Dashes indicate deleted nucleotides. Right panels, The Sanger-sequencing results. Two red lines and a vertical dashed black line indicate sites of nonhomologous end joining recombination. ***c***, Representative images of P0 pups are in ***d*** (see also Movie 1). ***d***, ***e***, The expression of miR-218 (***d***) in the midbrain of E14.5 KO embryos was evaluated by TaqMan assay. Data are normalized to the average of the reference sno-202 and represent the mean ± SEM of $2^{-\Delta Ct}$ values from 3 animals. *$p < 0.05$ (two-way ANOVA followed by Sidak). The expression of Slit2 and Slit3 (***e***) was evaluated in the midbrain of E14.5 WT and KO models by qPCR. Data are normalized to the average of the reference Hprt and represent the mean ± SEM of $2^{-\Delta Ct}$ values from three embryos. WT: miR-218-1$^{+/\pm}$; miR-218-2$^{+/\pm}$. KO1: miR-218-1$^{-/-}$; miR-218-2$^{+/\pm}$. KO2: miR-218-1$^{+/\pm}$; miR-218-2$^{-/-}$. dKO:

Table 1. Survival rate of the miR-218-1 and miR-218-2 KO mice

		Embryonal			Adult		
Mating	Genotype	No. of embryos	Observed frequency	Expected frequency	No. of animals	Observed frequency	Expected frequency
miR-218-1$^{+/-}$ × miR-218-1$^{+/-}$	miR-218-1$^{+/+}$	9	0.24	0.25	7	0.15	0.25
	miR-218-1$^{+/-}$	23	0.60	0.5	28	0.57	0.5
	miR-218-1$^{-/-}$	5	0.16	0.25	14	0.28	0.25
		Total 37	χ^2 test, $p = 0.217$		Total 49	χ^2 test, $p = 0.223$	
miR-218-2$^{+/-}$ × miR-218-2$^{+/-}$	miR-218-2$^{+/+}$	18	0.210	0.25	49	0.35	0.25
	miR-218-2$^{+/-}$	39	0.440	0.5	92	0.65	0.5
	miR-218-2$^{-/-}$	31	0.350	0.25	0	0	0.25
		Total 88	χ^2 test, $p = 0.083$		Total 141	χ^2 test, $p < 0.0001$	
miR-218-1$^{+/-}$-2$^{+/-}$ × miR-218-1$^{+/-}$-2$^{+/-}$	miR-218-1$^{+/+}$-2$^{+/+}$	1	0.030	0.0625	11	0.096	0.0625
	miR-218-1$^{+/+}$-2$^{+/-}$	3	0.091	0.125	22	0.193	0.125
	miR-218-1$^{+/+}$-2$^{-/-}$	2	0.061	0.0625	1	0.009	0.0625
	miR-218-1$^{+/+}$-2$^{-/-}$	5	0.152	0.125	20	0.175	0.125
	miR-218-1$^{+/-}$-2$^{+/-}$	10	0.303	0.25	37	0.325	0.25
	miR-218-1$^{+/-}$-2$^{-/-}$	8	0.242	0.125	1	0.009	0.125
	miR-218-1$^{-/-}$-2$^{+/+}$	1	0.030	0.0625	10	0.088	0.0625
	miR-218-1$^{-/-}$-2$^{+/-}$	2	0.061	0.125	13	0.114	0.125
	miR-218-1$^{-/-}$-2$^{-/-}$	1	0.030	0.0625	0	0.0	0.0625
		Total 33	χ^2 test, $p = 0.511$		Total 115	χ^2 test, $p < 0.0011$	

The number of observed animals for each genotype at both E14.5 (embryonal) and P0 (adult) stages obtained from different mating. χ2-test was used to compare observed and expected frequencies.

Movie 1. miR-218-1 and miR-218-2 KOs pups. The tail pinch response of newborn pups from control and miR-218 KO mice. From left to right they are: wild type, KO1, KO2 and dKO. [View online]

←

miR-218-1$^{-/-}$; miR-218-2$^{-/-}$. ***f***, The expression of Th in the midbrain of E14.5 KO embryos was evaluated by qPCR. Data are normalized to the average of the reference Hprt and represent the mean ± SEM of $2^{-\Delta Ct}$ values from three independent experiments. ***g***, Boxplot represents the percentage of TH-GFP^{+} DAn isolated from the midbrain of E14.5 KO embryos. ***h-k***, Immunostaining and quantifications for TH (***i***), PITX3 (***j***), and ISL1 (***k***) in the midbrain of E14.5 WT and double KO embryos. The count was performed from 10 randomly selected fields from at least three different litters for each condition. Images were acquired at 10× magnification. Scale bar, 100 μm. ***l-n***, Functional characterization of iDAn obtained from dKO E14 MEF. Current to voltage relationships of K^+ (***l***) and Na^+ (***m***) voltage-dependent currents, recorded in dKO and WT iDAn, elicited by depolarizing voltage steps (–40 to 40 mV, 5 mV increment, 300 ms) from VH = − 60 mV. A significant difference between dKO and WT iDAn is present for both I_{Na+} and I_{K+} current areas at most stimulus intensities. Data are mean ± SEM. *$p < 0.05$; **$p < 0.01$; ***$p < 0.001$; two-way repeated-measures ANOVA followed by Bonferroni test. ***n***, In current-clamp recordings, dKO iDAn fire a higher number of APs in response to depolarizing current injections (15-105 pA, 10 pA increment, 300 ms) compared with WT iDAn. Data are mean ± SEM. *$p < 0.05$; ***$p < 0.001$; two-way repeated-measures ANOVA, followed by Bonferroni test. iDAn were identified as TH-GFP^{+} cells.

deletion of miR-218-2 in the embryonic mesencephalon and rhombomere 1 (En1$^{+/Cre}$; miR-218-2$^{fl/fl}$, hereafter referred to as c-KO2), starting at approximately E9 (Gherbassi and Simon, 2020).

Midbrain specific double KO mice (miR-218-1$^{-/-}$; miR-218-2$^{fl/fl}$; En1$^{+/Cre}$; hereafter referred to as c-dKO) were viable, fertile, and showed no apparent defects in lifespan or fertility (Fig. 7*b*). The expression of miR-218 was specifically abolished in the adult midbrain from c-dKO mice at P39 (Fig. 7*c*). No significant changes were observed in the expression of miR-218-1 and miR-218-2 host genes, *Slit2* and *Slit3* (Fig. 7*d*,*e*). No alterations were observed in the expression of dopaminergic markers, such as *Th*, *Vmat2*, and *Dat* in adult animals (Fig. 7*f–h*). Additionally, the number of TH^{+} cells counted in c-KO2 sections (Fig. 7*i*,*j*), their density (Fig. 7*k*), and the percentage of positive pixel (Fig. 7*l*) were unchanged. Similarly, the total amount of TH protein (Fig. 7*m*) shows no differences, suggesting that there is no significant loss or degeneration in the dopaminergic population.

Next, we investigated the consequences of miR-218 deletion on the excitability of native DA neurons of the SNpc, the midbrain nucleus where the nigrostriatal dopaminergic pathway originates. To this purpose, we performed whole-cell patch-clamp recordings from SNpc DA neurons in *ex vivo* midbrain slices obtained from miR-218 KO1, cKO2, c-dKO, and WT adult TH-GFP^{+} mice. We found that membrane input resistance (R_m) was increased in all miR-218 single and double KO SNpc DAn compared with WT DAn, with the highest level of statistical significance for the miR-218 c-dKO group (Fig. 8*a*), indicating a clear dosage expression effect on the passive neuron membrane property. Spontaneous firing frequency, recorded in cell-attached configuration to avoid cytoplasm dialysis, was higher in KO1 (at the limit for statistical significance, $p = 0.052$) and c-KO2 ($p < 0.05$), but not in miR-218 c-dKO DAn (Fig. 8*b*). By contrast, the instantaneous frequency of APs evoked through depolarizing current injections (0-250 pA, 10 pA increment) was strongly augmented in c-dKO DA neurons, but not in single KO1 and c-KO2 DA neurons (Fig. 8*c*,*d*). The latter data were mirrored by a decrease of the minimal current necessary to evoke a single AP (rheobase), that resulted significantly lower than WT DAn in all single and double miR-218 KOs (Fig. 8*e*).

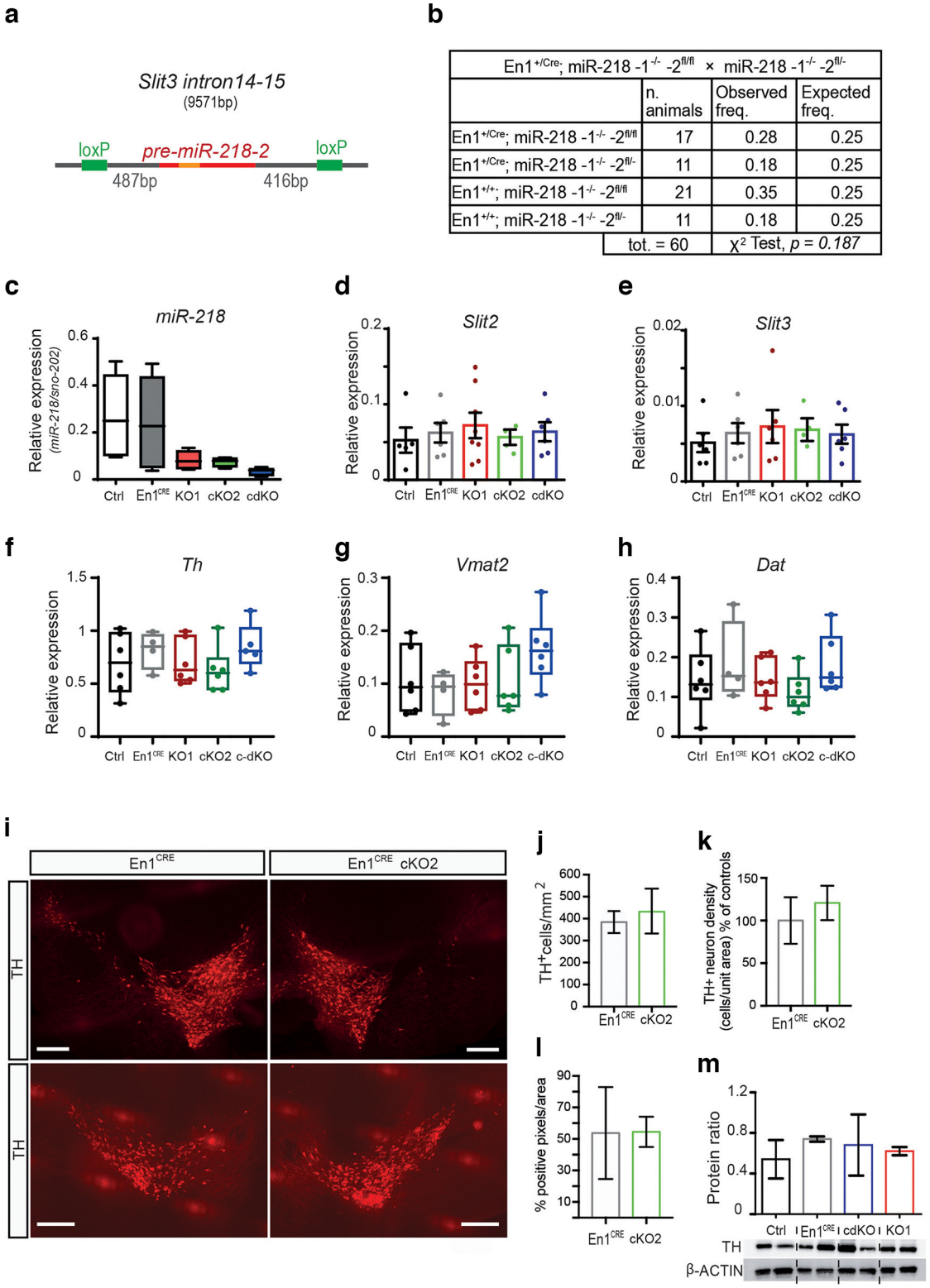

En1+/Cre; miR-218 -1-/- -2fl/fl × miR-218 -1-/- -2fl/-			
	n. animals	Observed freq.	Expected freq.
En1+/Cre; miR-218 -1-/- -2fl/fl	17	0.28	0.25
En1+/Cre; miR-218 -1-/- -2fl/-	11	0.18	0.25
En1+/+; miR-218 -1-/- -2fl/fl	21	0.35	0.25
En1+/+; miR-218 -1-/- -2fl/-	11	0.18	0.25
	tot. = 60	χ^2 Test, $p = 0.187$	

Figure 7. Midbrain specific deletion of miR-218. ***a***, Schematic representation of miR-218-$2^{fl/fl}$ allele generated through homologous recombination (for details, see Extended Data Fig. 7-1; Materials and Methods). ***b***, Survival rate of conditional double KO mice (c-dKO2). ***c***, TaqMan assay for the expression of miR-218 in the ventral midbrain of P39 WT, En1CRE, and miR-218 KO models. Data are normalized to the average of the reference sno-202 and represented as $2^{-\Delta Ct}$ values from 4 distinct animals. Median, interquartile range, and minimum and maximum are represented. *$p < 0.05$ with respect to Ctrl samples (Kruskal–Wallis test plus Dunn's multiple comparison correction). ***d***, ***e***, qPCR for midbrain expression of Slit2 (***b***) and Slit3 (***c***) in the ventral midbrain of P39 WT, $En1^{CRE}$, and miR-218 KO models. Data are normalized to the average of the reference Hprt and represent the mean ± SEM and all values of the $2^{-\Delta Ct}$ values from at least 4 animals. ***f–h***, The expression of the dopaminergic markers TH, VMAT2, and DAT in the ventral midbrain of P39 WT and KO mice was evaluated by qPCR. Data are normalized to the average of the reference Hprt and represent the median ± 2nd and 3rd quartile of $2^{-\Delta Ct}$ values from at least 3 different animals from three independent litters. ***i***, Representative images of TH^+ neurons in the ventral midbrain from control ($En1^{CRE}$) and $En1^{CRE}$ c-KO2 adult brain. Scale bar, 250 µm. ***j–l***, Quantification for the number of TH^+ cells (***j***), TH fluorescent density (***k***), and pixel intensity (***l***) does not show significant differences. ***m***, TH protein expression in the ventral midbrain of P39 WT, $En1^{CRE}$, and miR-218 KO models analyzed by Western blot. Data are normalized to the average of β-ACTIN and represent the mean ± SEM. $n = 3$. WT: miR-218-$1^{+/\pm}$; miR-218-$2^{+/\pm}$. KO1: miR-218-$1^{-/-}$; miR-218-$2^{+/\pm}$. KO2: miR-218-$1^{+/\pm}$; miR-218-$2^{-/-}$. dKO: miR-218-$1^{-/-}$; miR-218-$2^{-/-}$.

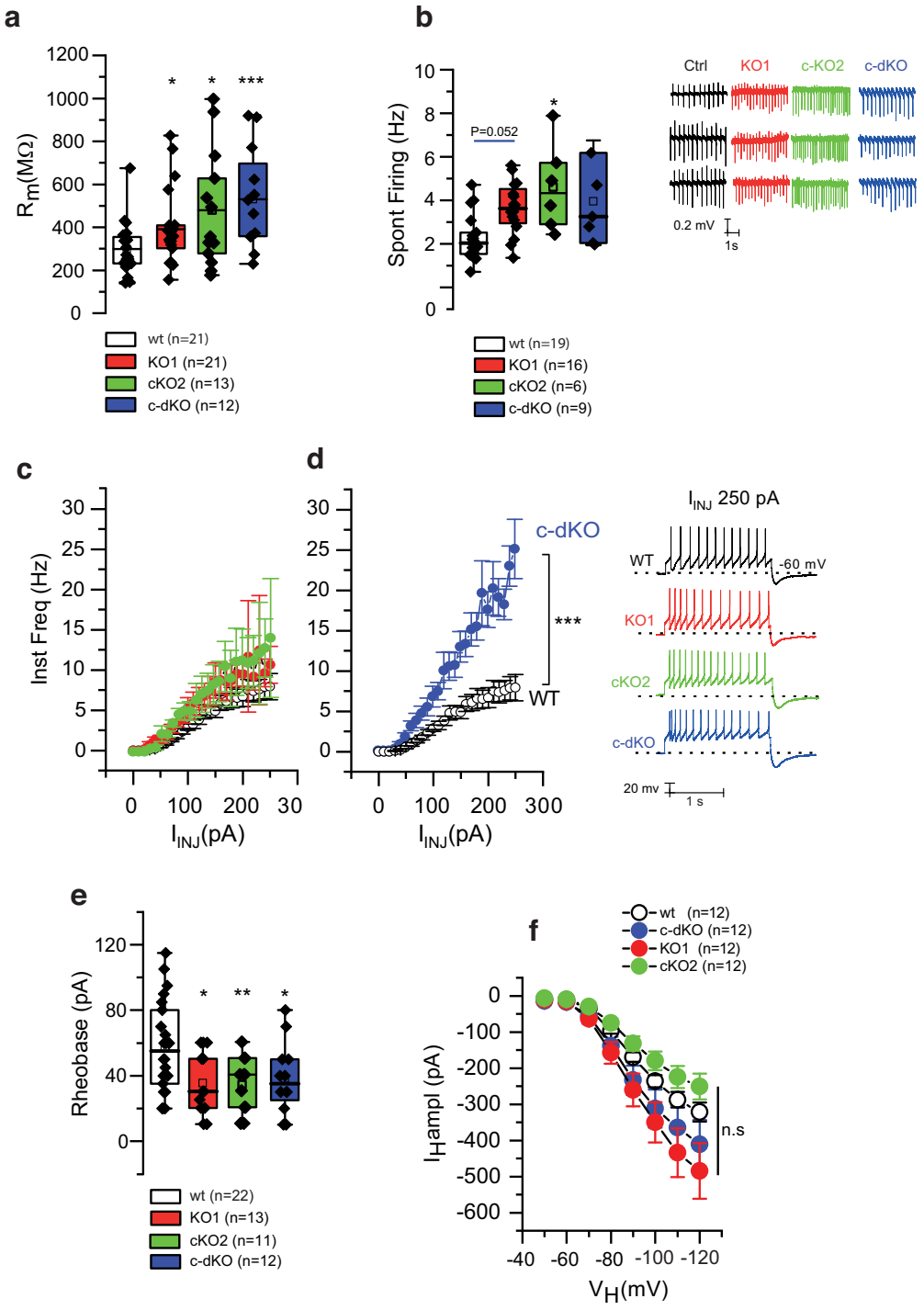

Figure 8. Electrical proprieties of DAn in SNpc of miR-218 KO mice. ***a-f***, Functional characterization of native DA neurons in *ex vivo* midbrain slices of WT, miR-218 KO1, c-KO2, and c-dKO adult mice. Active and passive membrane properties of DA neurons are controlled by miR-218 expression level. Deletion of miR-218 in KO1, c-KO2, and c-dKO strongly increases DA neurons membrane input resistance (R_m). Data are mean ± SEM. KO-1, $p < 0.05$; c-KO2, $p < 0.05$; c-dKO, $p < 0.001$; unpaired Student *t* test. ***a***, Spontaneous pacemaker firing in cell-attached recordings is significantly different only in c-KO2 WT DA neurons (***b***, box plot and example traces). KO-1, $p = 0.052$; c-KO2, $p < 0.05$, c-dKO, $p = 0.105$; unpaired Student *t* test. Evoked AP firing is severely modified in c-dKO DA neurons, which display hyperexcitability compared with WT, KO1, and c-KO2 DA neurons. Instantaneous frequency of the first two APs elicited by depolarizing currents (10-250 pA, 10 pA increment, 2 s) is dramatically increased in c-dKO versus WT DAn (***d***). 190 pA, $p < 0.05$; 240 pA, $p < 0.01$; 250 pA, $p < 0.001$; two-way repeated-measures ANOVA, followed by Bonferroni test. Data are mean ± SEM. Example traces of evoked firing refer to the highest stimulus intensity (250 pA) applied to WT, KO1, c-KO2, and c-dKO DA neurons (***d***, right). Rheobase is significantly lower in all groups (***e***). KO-1, $p < 0.05$; c-KO2, $p = 0.01$; c-dKO, $p < 0.05$; unpaired *t* test. The I_h current amplitude of WT, KO1, c-KO2, and c-dKO (***f***) was taken as the difference between the steady state (at the end of the 1 s pulse) and the current onset (at the start of the 1 s pulse) at −120 mV. I_h activation kinetics were calculated by fitting the current trace at −120 mV with a mixture of one or two standard exponential functions using Clampfit 9.

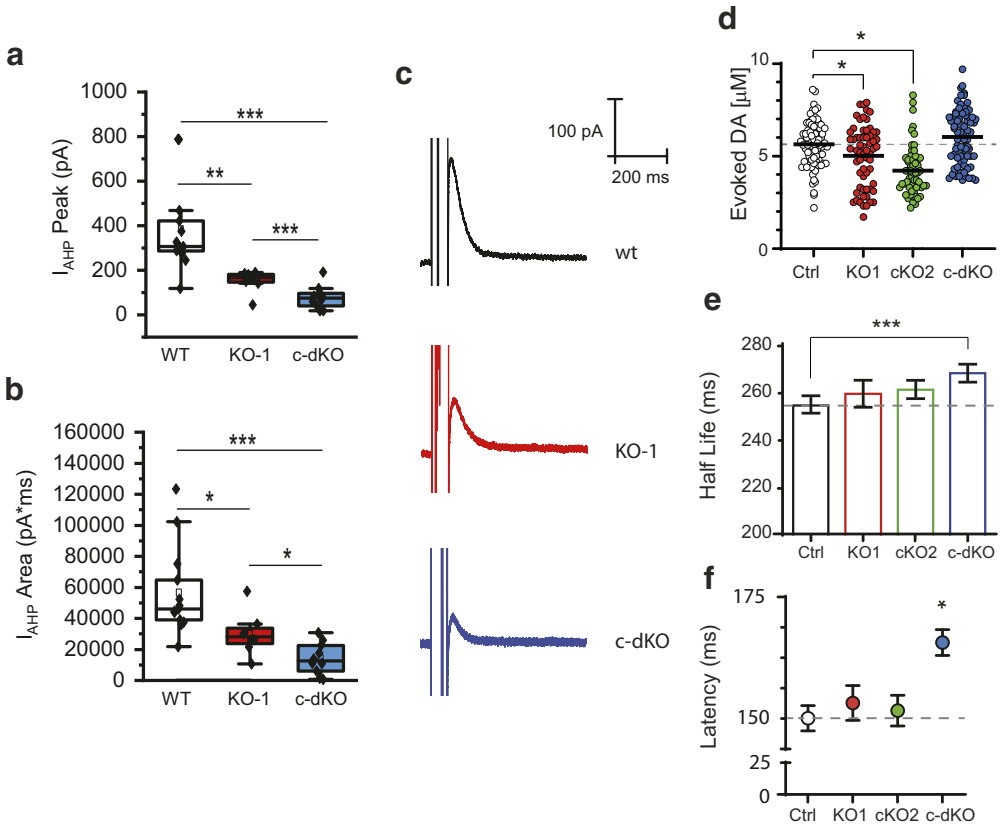

Figure 9. Deletion of miR-218 affects DA released. ***a–c***, Analysis of I_{AHP}. I_{AHP} peak (***a***) and area (***b***) elicited by a 100 ms voltage command to 0 mV is significantly reduced in KO-1 and c-dKO compared with WT DAn (I_{AHP} peak). KO-1, $p < 0.01$; c-dKO, $p < 0.001$; I_{AHP} area, KO-1, $p < 0.05$; c-dKO, $p < 0.001$; unpaired Student *t* test. Data are mean ± SEM. ***c***, Example traces of I_{AHP} in WT, KO-1, and c-dKO DAn showing a clear dosage expression effect of miR-218 onto I_{AHP}. ***d***, Maximal concentration (μM) of DA released in response to single rectangular electrical pulse, recorded by CPA, is significantly reduced in KO1 and c-KO2. KO-1, $p < 0.05$; KO-2, $p < 0.001$; but not in c-dKO striatal slices ($p = 0.067$); unpaired Student *t* test. Data are mean ± SEM. Uptake system(s) parameters, such as half-life time (***e***) and latency (***f***) of amperometric current, are increased selectively in c-dKO compared with WT striata ($p < 0.001$ and $p < 0.05$, respectively; unpaired *t* test), indicating that the complete miR-218 deletion reduces DA uptake efficacy.

Collectively, these data suggest that deletion of miR-218 causes an increase of intrinsic excitability of SNpc DAn.

To investigate the possible mechanism(s) underlying the hyperexcitability of DAn, we focused on two ionic conductances affecting their pacemaker firing. First, we analyzed the hyperpolarization-activated I_h current, a hallmark of DAn affecting firing activity (Friedman et al., 2014; Krashia et al., 2017). However, we found that I_h means amplitudes and *I–V* relationship were similar among all groups, suggesting that it is not responsible for the excitability change in the miR-218 KO DAn (Fig. 8*f*). Second, we measured the Ca^{2+}-activated K^+ current (Wolfart and Roeper, 2002), which underlies the I_{AHP} phase of each AP, thus affecting firing frequency and regularity in DAn (Deignan et al., 2012). We recorded I_{AHP} in KO1 and c-dKO DAn. In both genotypes, we found that I_{AHP} peak and area were strongly reduced compared with WT DAn with the highest level of statistical significance for c-dKO (Fig. 9*a–c*). Together, our data suggest that miR-218 expression controls either passive or active intrinsic membrane properties that heavily impact the neurophysiological characteristics of SNpc DA neurons.

Based on these observations, we hypothesized that the altered intrinsic excitability of DAn could impair their ability to release DA in the target areas. To test this, we performed CPA recordings (Federici et al., 2014; Guatteo et al., 2017) in dorsolateral striatum slices from adult mice in the four experimental groups. The maximal amplitudes of the DA efflux in response to a single electrical stimulus of the dopaminergic fibers were reduced in KO1 and c-KO2, but not in c-dKO, compared with WT dorsolateral striatum (Fig. 9*d*). The discrepancy observed in c-dKO slices was paralleled by an increase in the amperometric signal half-life and latency, two parameters strongly influenced by DA reuptake systems, which were not altered in single KO striatal slices (Fig. 9*e*,*f*).

miR-218 controls the expression of synaptic specific genes

To understand how deletion of miR-218 affects dopamine release and neuronal excitability, we searched for upregulated genes in miR-218 KO mice, compared with control animals. We first combined four distinct algorithms (TargetScan8.0, DIANA microT-CDS, mirBD, and PicTar) to identify all miR-218 target genes hosting a potential miR-218 binding site in their 3′UTR sequence. This approach allowed us to identify 163 potential targets for the miR-218 (Extended Data Fig. 10-1*a*). These genes appear strongly associated with synaptic activity, as revealed by GO analysis, where of the top 20 terms for Cellular Component (GO:CC), 9 terms refer directly to the synapse and 7 others are related to the synapse (as dendritic compartment and axon) (Fig. 10*a*; Extended Data Fig. 10-1*b*). Similar results came out when we performed the analysis for the Biological Process (GO:BP), where exocytosis and synaptic transmission resulted on top of the list (Extended Data Fig. 10-1*c*).These processes are specific to miR-218 since a similar analysis performed on three other microRNAs known to be involved in DAn development and function: miR-29a, miR-

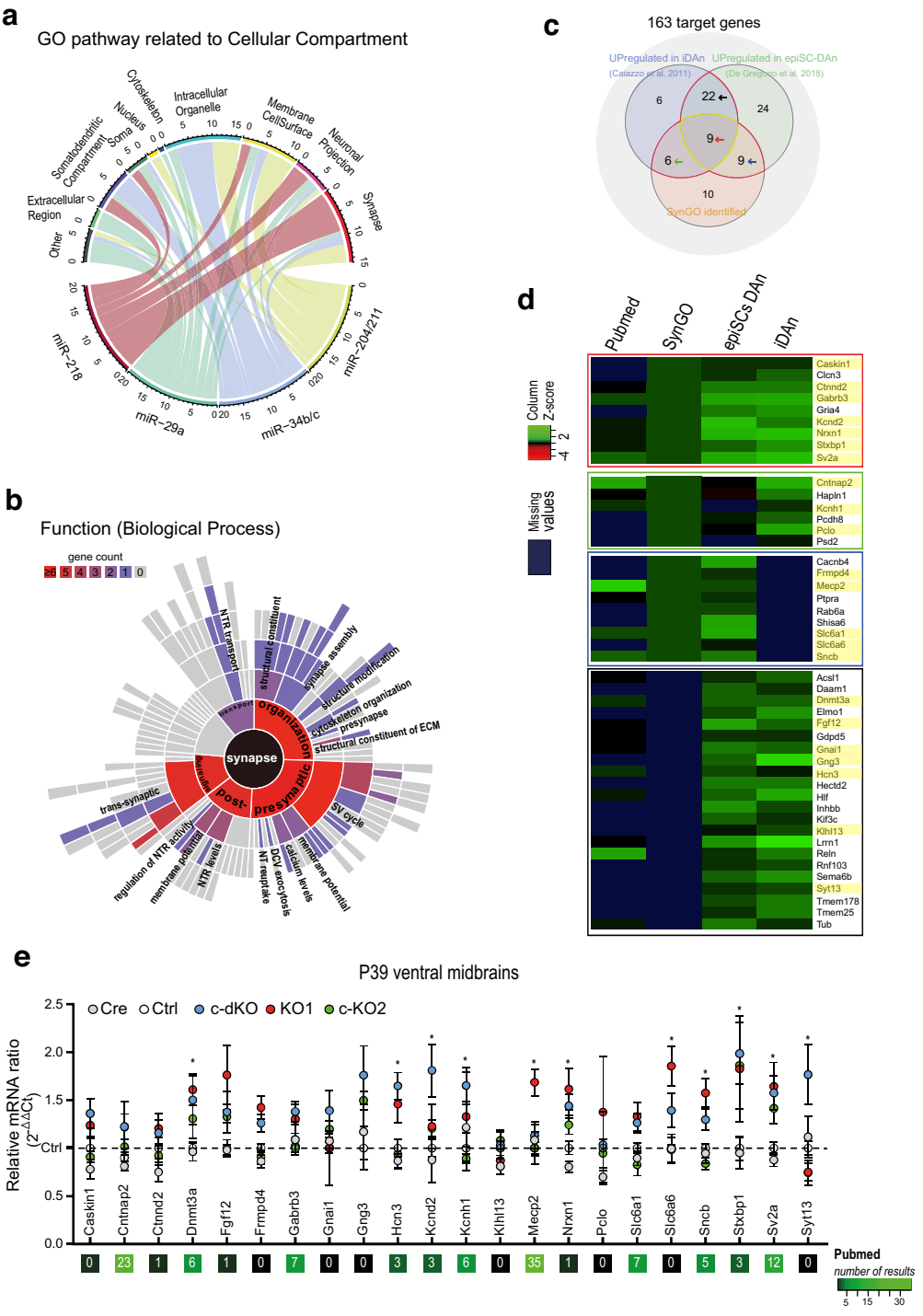

Figure 10. miR-218 regulates synaptic related genes. ***a***, Chord diagram clustering the top 20 GO:*CC* enriched terms for miR-218, miR-29a, miR-34b/c, and miR-204/211 reported in Extended Data Figure 10-1. ***b***, Diagram represents the SynGO:*BP* enriched terms for the miR-218's targets. The list of annotated genes is reported in Extended Data Figure 10-2. ***c***, Venn diagram that groups miR-218 target genes on the basis of their expression in episC-derived and MEF-derived DAn. And for their annotation as synaptic related in SynGO. ***d***, Magnification of heatmap in Extended Data Figure 10-2 for the selected genes. ***e***, qPCR analysis for the expression of selected miR-218's target genes in the ventral midbrain of P39 WT and cKO mice. Data were normalized to the average of the reference Hprt and related to the expression levels of Ctrl (=1), and represent the mean ± SEM of $2^{-\Delta\Delta Ct}$ values from at least 3 distinct animals. *$p < 0.05$ of at least one of one of KO samples with respect to the Ctrl (two way-ANOVA plus Dunn's *post hoc*).

34b/c-5p, and miR-204/211-5p (Volpicelli et al., 2019; Pulcrano et al., 2022) identified different cellular components, mostly correlated to somatodendritic compartments and organelles (Fig. 10*a*; Fig. Extended Data Fig. 10-1*d-l*). To further validate the involvement of miR-218 predicted targets in synaptic related functions, we checked whether the 163 candidates were annotated in the Syn-GO database, which is evidence-based and focused on synaptic activity regulation (Koopmans et al., 2019). We found that 34 genes were robustly annotated as involved in the regulation of synaptic activity and organization at both presynaptic and postsynaptic terminal (Fig. 10*b*; Extended Data Fig. 10-2, see table).

Additionally, we analyzed the expression of the 163 targets in mature functional DAn using previously published datasets

obtained from DAn derived from Pitx3-GFP epiSC (Jaeger et al., 2011; De Gregorio et al., 2018) and iDAn derived from transdifferentiated MEFs (Caiazzo et al., 2011). This analysis narrowed down the list to 24 genes that were both annotated in SynGo and expressed in DAn by at least one of the two datasets and 22 genes that were not identified as synaptic related by SynGO but were upregulated in both datasets (Fig. 10*c*; Extended Data Fig. 10-2*a*, *b*). Interestingly, only 23 of these 46 have been previously associated with DAn or miR-218 signaling, or membrane excitability, while 24 were found to be part of the same functional network based on the STRING database (https://string-db.org/; Extended Data Fig. 10-3). By combining these approaches, we examined the expression of 22 transcripts in the ventral midbrains of P39 WT, KO1, c-KO2, and c-dKO mice (Fig. 10*d*). We observed significant upregulation (two way-ANOVA plus Dunn's *post hoc*) of the following genes: *Dnmt3a, Hcn3, Mecp2, Nrxn1, Slc6a6, Sncb, Stxbp1, Sv2a, Syt13* in miR-218 KO-*1*; *Hcn3, Kcnd2, Kcnh1, Stxbp1, Sv2a* in *miR-218 c-KO2*; and *Stxbp1* and *Sv2a* in miR-218 c-dKO (Fig. 10*e*). While *Stxbp1* and *Sv2a* were upregulated in all KO models, alteration in the expression of other candidates appeared to be specific to each mutant indicating a complex pathway of interactions.

Discussion

microRNA are fine regulators of protein expression, and their dysregulation can affect the molecular composition and functional characteristics of brain networks (Brennan and Henshall, 2020). Manipulation of miR-218 levels has been shown to impact the functional activity and morphology of various neuronal subtypes, including motor neurons of the spinal cord and hippocampal neurons (Amin et al., 2015; Lu et al., 2021). The involvement of miR-218 in the biology of DAn is well documented (Baek et al., 2014; Cuesta et al., 2018), and mutations affecting the expression of miR-218 have been associated with motor neuron, and depression-related disorders (Cerro-Herreros et al., 2018, 2021; Reichenstein et al., 2019; Jurkiewicz et al., 2020). In addition multi-omics approaches have identified miR-218 as a relevant deregulated gene in a cohort of Parkinsonian patients (Li et al., 2018; Caldi Gomes et al., 2022).

Here we demonstrate, for the first time, that miR-218 is expressed in mesencephalic DAn where it promotes dopaminergic differentiation either alone or in combination with pro-dopaminergic transcription factors. This highlights its potential use to enhance the yield *in vitro* of DAn, particularly for cellular transplantation approaches that have recently emerged as potential treatment for Parkinson's disease (Parmar et al., 2020). The evidence that iDAn generated from dKO mice fibroblasts do not show differences in the expression of dopaminergic markers, but only in their activity, points to a functional rather than developmental role for miR-218, as reported for other miRNAs (Tan et al., 2013; Rajman et al., 2017). However, the mechanism behind the role of miR-218 in committing cells toward DAn differentiation remains unclear, and current knowledge suggests that miR-218 is involved in the transition from the immature to mature functional neurons (Pons-Espinal et al., 2017) by suppressing alternative differentiation processes (Amin et al., 2015).

The electrophysiological analysis provides insight into its role as a regulator of various neurophysiological parameters in DAn. Deletion of either a single or both isoform of miR-218 increases membrane input resistance, which is a passive membrane property influenced by the complement of ion channels expressed by neurons. For instance, downregulation of leak channels in miR-218 KO DAn or alteration in synaptic inputs and/or dendritic complexity may also affect membrane input resistance in neurons (Al-Muhtasib et al., 2018). Although these parameters were not explored in this study, miR-218 KO-2 CA1 hippocampal neurons exhibit reduced dendritic length and complexity (Lu et al., 2021), which correlates with higher membrane input resistance in DAn (Ledonne et al., 2023) and striatal neurons (Al-Muhtasib et al., 2018).

The most significant increase in the instantaneous frequency of evoked AP was observed in miR-218 c-dKO DAn, despite that this group did not show an overt increase in spontaneous firing. In c-dKO Dan, we found a marked reduction in the Ca^{2+}-activated K^+ conductance, an ionic current strongly affecting DAn firing. This current includes a pure Ca^{2+}-activated K^+ conductance (small conductance channels) and a Ca^{2+}- and voltage-dependent K^+ conductance (big conductance channels) (Gantz et al., 2018). Both currents underlie the I_{AHP} phase of each AP, and their reduction strongly increases the number of evoked APs in DAn of a Parkinson's disease rat model (Ledonne et al., 2023). Deletion of miR-218 may reduce I_{AHP} by different mechanisms, such as limiting free Ca^{2+} ion concentration or directly affecting the expression/function of the channels involved. The observed changes in DAn excitability align with previous evidence showing that miR-218-1 and miR-218-2 downregulate the expression of genes involved in neurotransmission (Amin et al., 2015), resulting in hyperexcitability in spinal cord neurons. Our results suggest that miR-218 also plays a role in controlling cellular excitability in midbrain DAn by regulating passive and active membrane electrical properties of these neurons.

The reduction in the release of dopamine could be attributed to different factors. In single KOs, the higher tonic (spontaneous) firing of the DAn might deplete the releasable DA vesicle pool or reduce the size and number of synaptic vesicles located in the synapse active zones, as recently reported for the glutamatergic synapses in miR-218 KO2 CA1 hippocampal neurons (Lu et al., 2021). Surprisingly, the evoked dopamine release in c-dKO is similar to that recorded in WT striata. However, in c-dKO striatal slices, the half lifetime and latency of the amperometric signal, which reflect the uptake systems efficacy of released dopamine (Federici et al., 2014), were both altered. This suggests that complete deletion of miR-218 may affect the reuptake of dopamine and indirectly compensate for the reduction of dopamine release, although no differences were observed in the mRNA level for the dopamine transporter *Dat*. Other factors, such as post-transcriptional regulations, induced by abnormal stimulation of dopamine D2 and D3 receptors followed by ubiquitination and degradation could regulate DAT activity (Luis-Ravelo et al., 2021). The differences in dopamine release among miR-218 KO1, c-KO2, and c-dKO might be related to a dosage–response effect, similarly to what has been described in motor neurons (Amin et al., 2021), where modulation of miR-218 levels leads to nonratiometric regulatory outputs on multiple miR-218 targets.

Through a comprehensive and systematic analysis, we have identified a subset of targets that are upregulated in miR-218 KO1, KO2, and c-dKO mice. Among these, *Sv2a* is of particular interest as it has been associated with neurotransmitter release at the synapses (Nowack et al., 2010; Wan et al., 2010) and its homolog *Sv2c* associated with Parkinson's disease and dopamine release (Dunn et al., 2017). *Sv2a* and most of the identified targets cluster as components of the synapse, although some are primarily involved in the regulation of gene expression at the synapse. This is the case with *Dnmt3a* and *Mecp2*, whose

expression was significantly upregulated in the midbrain of miR-218 KO1 mice. These genes are known as epigenetic regulators in the brain (Clemens and Gabel, 2020). Interestingly, the biological process, "Regulation of gene expression, epigenetic" (GO:0040029) emerges among the top 3 when clustering all 163 potential targets of miR-218. Thus, an intriguing possibility suggests that miR-218 may fine-tune a subset of synaptic related genes through the regulation of epigenetic mechanisms (Yan et al., 2017) as seen with other miRNAs (Swahari et al., 2021). Notably, overexpression of *Dnmt3a* leads to a phenotype of hyperexcitability similar to what we observed in miR-218 c-dKO (Cui et al., 2020; Li et al., 2022) and Dnmt3a-mediated methylation controls the expression of many synaptic related genes (Swahari et al., 2021).

Although we did not identify a significant impact of miR-218 on DAn survival, despite speculation about its potential effects, it should be noted that rodent DAn are known to be more resistant to degeneration compared with human DAn, and existing animal models attempting to replicate Parkinson's disease-associated dopaminergic degeneration have struggled to accurately reproduce the degenerative process (Dauer and Przedborski, 2003). Conducting a more comprehensive analysis throughout the lifespan of miR-218 KO animals, with a focus on older animals, that may be more susceptible to dopaminergic degeneration, could help uncover potential dopaminergic-related phenotypes.

The perinatal lethality observed in miR-218-2 KO mice, but not in miR-218-1, is intriguing given the widespread expression of both isoforms in the nervous system, although a detailed analysis on miR-218s expression in different brain regions throughout development is missing. We may hypothesize that miR-218-2 is able to compensate for the absence of miR-218-1, while the reverse may not be true, or that miR-218-1 and miR-218-2 control distinct gene networks associated with synaptic function, leading to different phenotypic outcomes. However, obtaining definitive evidence for these explanations is currently challenging. One potential approach to further investigate these hypotheses is the application of exogenous miR-218 precursors to attempt to rescue the phenotypes observed in single KO mice, but delivering miRNAs to the dopaminergic system poses challenges because of the midbrain's location. Alternatively, *ex vivo* approaches using organotypic slices could provide valuable insights into the effects of exogenous miR-218 on synaptic function and possible phenotypic rescue. Exploring the potential therapeutic use of miR-218 for other neurodegenerative disorders is worth considering, and further research in this direction could shed light on the therapeutic potential of miR-218 and its application in treating neurodegenerative diseases.

Achieving the specific deletion of miR-218-2 in different brain regions will provide the opportunity to distinguish phenotypic impairments directly associated with DAn from those associated with other neuronal subtypes, including motoneurons. Addressing this effect could be accomplished through the use of specific Cre deletion strategies. Thus, the conditional allele generated for miR-218-2 enables the investigation of related synaptic dysfunctions beyond the dopaminergic system.

Additionally, studying mutations affecting mature miR-218 or its precursor and their association with human-related defects, as observed in motor neuron-related disorders (Reichenstein et al., 2019), could provide valuable insights. The capacity of miR-218 to promote DAn differentiation holds potential in mitigating DAn loss, enhancing cell survival, and facilitating differentiation in Parkinson's disease patients. Thus, the use of miRNA-like sequences could emerge as a possible strategy for treating specific human disorders, although further basic research is necessary to provide additional support for these concepts.

References

Acampora D, Mazan S, Lallemand Y, Avantaggiato V, Maury M, Simeone A, Brûlet P (1995) Forebrain and midbrain regions are deleted in Otx2$^{-/-}$ mutants due to a defective anterior neuroectoderm specification during gastrulation. Development 121:3279–3290.

Acampora D, Di Giovannantonio LG, Di Salvio M, Mancuso P, Simeone A (2009) Selective inactivation of Otx2 mRNA isoforms reveals isoform-specific requirement for visceral endoderm anteriorization and head morphogenesis and highlights cell diversity in the visceral endoderm. Mech Dev 126:882–897.

Agarwal V, Bell GW, Nam JW, Bartel DP (2015) Predicting effective microRNA target sites in mammalian mRNAs. Elife 4:e05005.

Al-Muhtasib N, Forcelli PA, Vicini S (2018) Differential electrophysiological properties of D1 and D2 spiny projection neurons in the mouse nucleus accumbens core. Physiol Rep 6:e13784.

Alwin Prem Anand A, Alvarez-Bolado G, Wizenmann A (2020) MiR-9 and the midbrain-hindbrain boundary: a showcase for the limited functional conservation and regulatory complexity of microRNAs. Front Cell Dev Biol 8:586158.

Amin ND, et al. (2015) Loss of motoneuron-specific microRNA-218 causes systemic neuromuscular failure. Science 350:1525–1529.

Amin ND, Senturk G, Costaguta G, Driscoll S, O'Leary B, Bonanomi D, Pfaff SL (2021) A hidden threshold in motor neuron gene networks revealed by modulation of miR-218 dose. Neuron 109:3252–3267.e6.

Antoniou A, Khudayberdiev S, Idziak A, Bicker S, Jacob R, Schratt G (2018) The dynamic recruitment of TRBP to neuronal membranes mediates dendritogenesis during development. EMBO Rep 19:e44853.

Aversa D, Martini A, Guatteo E, Pisani A, Mercuri NB, Berretta N (2018) Reversal of dopamine-mediated firing inhibition through activation of the dopamine transporter in substantia nigra pars compacta neurons. Br J Pharmacol 175:3534–3547.

Baek S, Choi H, Kim J (2014) Ebf3-miR218 regulation is involved in the development of dopaminergic neurons. Brain Res 1587:23–32.

Bartel DP (2004) MicroRNAs: genomics, biogenesis, mechanism, and function. Cell 116:281–297.

Brennan GP, Henshall DC (2020) MicroRNAs as regulators of brain function and targets for treatment of epilepsy. Nat Rev Neurol 16:506–519.

Caiazzo M, Dell'Anno MT, Dvoretskova E, Lazarevic D, Taverna S, Leo D, Sotnikova TD, Menegon A, Roncaglia P, Colciago G, Russo G, Carninci P, Pezzoli G, Gainetdinov RR, Gustincich S, Dityatev A, Broccoli V (2011) Direct generation of functional dopaminergic neurons from mouse and human fibroblasts. Nature 476:224–227.

Caldi Gomes L, Galhoz A, Jain G, Roser AE, Maass F, Carboni E, Barski E, Lenz C, Lohmann K, Klein C, Bähr M, Fischer A, Menden MP, Lingor P (2022) Multi-omic landscaping of human midbrains identifies disease-relevant molecular targets and pathways in advanced-stage Parkinson's disease. Clin Transl Med 12:e692.

Cerro-Herreros E, Sabater-Arcis M, Fernandez-Costa JM, Moreno N, Perez-Alonso M, Llamusi B, Artero R (2018) miR-23b and miR-218 silencing increase Muscleblind-like expression and alleviate myotonic dystrophy phenotypes in mammalian models. Nat Commun 9:2482.

Cerro-Herreros E, González-Martínez I, Moreno N, Espinosa-Espinosa J, Fernández-Costa JM, Colom-Rodrigo A, Overby SJ, Seoane-Miraz D, Poyatos-García J, Vilchez JJ, López de Munain A, Varela MA, Wood MJ, Pérez-Alonso M, Llamusí B, Artero R (2021) Preclinical characterization of antagomiR-218 as a potential treatment for myotonic dystrophy. Mol Ther Nucleic Acids 26:174–191.

Chang SH, Su YC, Chang M, Chen JA (2021) MicroRNAs mediate precise control of spinal interneuron populations to exert delicate sensory-to-motor outputs. Elife 10:e63768.

Clemens AW, Gabel HW (2020) Emerging insights into the distinctive neuronal methylome. Trends Genet 36:816–832.

Colameo D, Rajman M, Soutschek M, Bicker S, von Ziegler L, Bohacek J, Winterer J, Germain PL, Dieterich C, Schratt G (2021) Pervasive compartment-specific regulation of gene expression during homeostatic synaptic scaling. EMBO Rep 22:e52094.

Cucchiaroni ML, Freestone PS, Berretta N, Viscomi MT, Bisicchia E, Okano H, Molinari M, Bernardi G, Lipski J, Mercuri NB, Guatteo E (2011) Properties of dopaminergic neurons in organotypic mesencephalic-striatal co-cultures: evidence for a facilitatory effect of dopamine on the glutamatergic input mediated by α-1 adrenergic receptors. Eur J Neurosci 33:1622–1636.

Cuesta S, Restrepo-Lozano JM, Silvestrin S, Nouel D, Torres-Berrío A, Reynolds LM, Arvanitogiannis A, Flores C (2018) Non-contingent exposure to amphetamine in adolescence recruits miR-218 to regulate Dcc expression in the VTA. Neuropsychopharmacology 43:900–911.

Cui D, Mesaros A, Burdeos G, Voigt I, Giavalisco P, Hinze Y, Purrio M, Neumaier B, Drzezga A, Obata Y, Endepols H, Xu X (2020) Dnmt3a2/Dnmt3L overexpression in the dopaminergic system of mice increases exercise behavior through signaling changes in the hypothalamus. Int J Mol Sci 21:6297.

De Gregorio R, Pulcrano S, De Sanctis C, Volpicelli F, Guatteo E, von Oerthel L, Latagliata EC, Esposito R, Piscitelli RM, Perrone-Capano C, Costa V, Greco D, Puglisi-Allegra S, Smidt MP, di Porzio U, Caiazzo M, Mercuri NB, Li M, Bellenchi GC (2018) miR-34b/c regulates Wnt1 and enhances mesencephalic dopaminergic neuron differentiation. Stem Cell Reports 10:1237–1250.

Deignan J, Luján R, Bond C, Riegel A, Watanabe M, Williams JT, Maylie J, Adelman JP (2012) SK2 and SK3 expression differentially affect firing frequency and precision in dopamine neurons. Neuroscience 217:67–76.

Deng Q, Andersson E, Hedlund E, Alekseenko Z, Coppola E, Panman L, Millonig JH, Brunet JF, Ericson J, Perlmann T (2011) Specific and integrated roles of Lmx1a, Lmx1b and Phox2a in ventral midbrain development. Development 138:3399–3408.

di Porzio U, Daguet MC, Glowinski J, Prochiantz A (1980) Effect of striatal cells on in vitro maturation of mesencephalic dopaminergic neurones grown in serum-free conditions. Nature 288:370–373.

di Val Cervo PR, Romanov RA, Spigolon G, Masini D, Martín-Montañez E, Toledo EM (2017) Induction of functional dopamine neurons from human astrocytes in vitro and mouse astrocytes in a Parkinson's disease model. Nat Biotechnol 40:1–12.

Dauer W, Przedborski S (2003) Parkinson's disease: mechanisms and models. Neuron 39:889–909.

Dunn AR, Stout KA, Ozawa M, Lohr KM, Hoffman CA, Bernstein AI, Li Y, Wang M, Sgobio C, Sastry N, Cai H, Caudle WM, Miller GW (2017) Synaptic vesicle glycoprotein 2C (SV2C) modulates dopamine release and is disrupted in Parkinson disease. Proc Natl Acad Sci USA 114:E2253–E2262.

Federici M, Latagliata EC, Ledonne A, Rizzo FR, Feligioni M, Sulzer D, Dunn M, Sames D, Gu H, Nisticò R, Puglisi-Allegra S, Mercuri NB (2014) Paradoxical abatement of striatal dopaminergic transmission by cocaine and methylphenidate. J Biol Chem 289:264–274.

Friedman AK, Walsh JJ, Juarez B, Ku SM, Chaudhury D, Wang J, Li X, Dietz DM, Pan N, Vialou VF, Neve RL, Yue Z, Han MH (2014) Enhancing depression mechanisms in midbrain dopamine neurons achieves homeostatic resilience. Science 344:313–319.

Gantz SC, Ford CP, Morikawa H, Williams JT (2018) The evolving understanding of dopamine neurons in the substantia nigra and ventral tegmental area. Annu Rev Physiol 80:219–241.

Ge SX, Jung D, Yao R (2020) ShinyGO: a graphical gene-set enrichment tool for animals and plants. Bioinformatics 36:2628–2629.

Gherbassi D, Simon HH (2006) The engrailed transcription factors and the mesencephalic dopaminergic neurons. J Neural Transm Suppl 47–55.

Guatteo E, Yee A, McKearney J, Cucchiaroni ML, Armogida M, Berretta N, Mercuri NB, Lipski J (2013) Dual effects of L-DOPA on nigral dopaminergic neurons. Exp Neurol 247:582–594.

Guatteo E, Rizzo FR, Federici M, Cordella A, Ledonne A, Latini L, Nobili A, Viscomi MT, Biamonte F, Landrock KK, Martini A, Aversa D, Schepisi C, D'Amelio M, Berretta N, Mercuri NB (2017) Functional alterations of the dopaminergic and glutamatergic systems in spontaneous α-synuclein overexpressing rats. Exp Neurol 287:21–33.

Huang T, Liu Y, Huang M, Zhao X, Cheng L (2010) Wnt1-cre-mediated conditional loss of Dicer results in malformation of the midbrain and cerebellum and failure of neural crest and dopaminergic differentiation in mice. J Mol Cell Biol 2:152–163.

Jaeger I, Arber C, Risner-Janiczek JR, Kuechler J, Pritzsche D, Chen IC, Naveenan T, Ungless MA, Li M (2011) Temporally controlled modulation of FGF/ERK signaling directs midbrain dopaminergic neural progenitor fate in mouse and human pluripotent stem cells. Development 138:4363–4374.

Jurkiewicz M, Moser D, Koller A, Yu L, Chen EI, Bennett DA, Canli T (2020) Integration of postmortem amygdala expression profiling, GWAS, and functional cell culture assays: neuroticism-associated synaptic vesicle glycoprotein 2A (SV2A) gene is regulated by miR-133a and miR-218. Transl Psychiatry 10:297.

Kanehisa M, Goto S, Furumichi M, Tanabe M, Hirakawa M (2010) KEGG for representation and analysis of molecular networks involving diseases and drugs. Nucleic Acids Res 38:D355–D360.

Koopmans F, et al. (2019) SynGO: an evidence-based, expert-curated knowledge base for the synapse. Neuron 103:217–234.e4.

Kimmel RA, Turnbull DH, Blanquet V, Wurst W, Loomis CA, Joyner AL (2000) Two lineage boundaries coordinate vertebrate apical ectodermal ridge formation. Genes Dev 14:1377–1389.

Krashia P, Martini A, Nobili A, Aversa D, D'Amelio M, Berretta N, Guatteo E, Mercuri NB (2017) On the properties of identified dopaminergic neurons in the mouse substantia nigra and ventral tegmental area. Eur J Neurosci 45:92–105.

Krek A, et al. (2005) Combinatorial microRNA target predictions. Nat Genet 37:495–500.

Ledonne A, Massaro Cenere M, Paldino E, D'Angelo V, D'Addario SL, Casadei N, Nobili A, Berretta N, Fusco FR, Ventura R, Sancesario G, Guatteo E, Mercuri NB (2023) Morpho-functional changes of nigral dopamine neurons in an α-synuclein model of Parkinson's disease. Mov Disord 38:256–266.

Li J, Sun Y, Chen J (2018) Identification of critical genes and miRNAs associated with the development of Parkinson's disease. J Mol Neurosci 65:527–535.

Li J, Pinto-Duarte A, Zander M, Cuoco MS, Lai CY, Osteen J, Fang L, Luo C, Lucero JD, Gomez-Castanon R, Nery JR, Silva-Garcia I, Pang Y, Sejnowski TJ, Powell SB, Ecker JR, Mukamel EA, Behrens MM (2022) Dnmt3a knockout in excitatory neurons impairs postnatal synapse maturation and increases the repressive histone modification H3K27me3. Elife 11:e66909.

Livak KJ, Schmittgen TD (2001) Analysis of relative gene expression data using real-time quantitative PCR and the 2(-Delta Delta C(T)) method. Methods 25:402–408.

Lu SY, et al. (2021) miR-218-2 regulates cognitive functions in the hippocampus through complement component 3-dependent modulation of synaptic vesicle release. Proc Natl Acad Sci USA 118:e2021770118.

Luis-Ravelo D, Fumagallo-Reading F, Castro-Hernandez J, Barroso-Chinea P, Afonso-Oramas D, Febles-Casquero A, Cruz-Muros I, Salas-Hernandez J, Mesa-Infante V, Rodriguez-Nuñez J, Gonzalez-Hernandez T (2021) Prolonged dopamine D3 receptor stimulation promotes dopamine transporter ubiquitination and degradation through a PKC-dependent mechanism. Pharmacol Res 165:105434.

Martinez-Morales JR, Signore M, Acampora D, Simeone A, Bovolenta P (2001) Otx genes are required for tissue specification in the developing eye. Development 128:2019–2030.

Martin KC, Ephrussi A (2009) mRNA localization: gene expression in the spatial dimension. Cell 136:719–730.

Martini A, Cordella A, Pisani A, Mercuri NB, Guatteo E (2019) Neurotensin receptors inhibit mGluR I responses in nigral dopaminergic neurons via a process that undergoes functional desensitization by G-protein coupled receptor kinases. Neuropharmacology 155:76–88.

Mercuri NB, Bonci A, Pisani A, Calabresi P, Bernardi G (1995) Actions of glycine on non-dopaminergic neurons of the rat substantia nigra. Eur J Neurosci 7:2351–2354.

Nobili A, et al. (2017) Dopamine neuronal loss contributes to memory and reward dysfunction in a model of Alzheimer's disease. Nat Commun 8:14727.

Nowack A, Yao J, Custer KL, Bajjalieh SM (2010) SV2 regulates neurotransmitter release via multiple mechanisms. Am J Physiol Cell Physiol 299:C960–C967.

Pang X, Hogan EM, Casserly A, Gao G, Gardner PD, Tapper AR (2014) Dicer expression is essential for adult midbrain dopaminergic neuron maintenance and survival. Mol Cell Neurosci 58:22–28.

Paraskevopoulou MD, Georgakilas G, Kostoulas N, Vlachos IS, Vergoulis T, Reczko M, Filippidis C, Dalamagas T, Hatzigeorgiou AG (2013) DIANA-MicroT Web Server v5.0: service integration into miRNA functional analysis workflows. Nucleic Acids Res 41:W169–W173.

Parmar M, Li M (2007) Early specification of dopaminergic phenotype during ES cell differentiation. BMC Dev Biol 7:86.

Parmar M, Grealish S, Henchcliffe C (2020) The future of stem cell therapies for Parkinson disease. Nat Rev Neurosci 21:103–115.

Pons-Espinal M, de Luca E, Marzi MJ, Beckervordersandforth R, Armirotti A, Nicassio F, Fabel K, Kempermann G, De Pietri Tonelli D (2017) Synergic functions of miRNAs determine neuronal fate of adult neural stem cells. Stem Cell Reports 8:1046–1061.

Prochiantz A, di Porzio U, Kato A, Berger B, Glowinski J (1979) In vitro maturation of mesencephalic dopaminergic neurons from mouse embryos is enhanced in presence of their striatal target cells. Proc Natl Acad Sci USA 76:5387–5391.

Puelles E, Acampora D, Lacroix E, Signore M, Annino A, Tuorto F, Filosa S, Corte G, Wurst W, Ang SL, Simeone A (2003) Otx dose-dependent integrated control of antero-posterior and dorso-ventral patterning of midbrain. Nat Neurosci 6:453–460.

Pulcrano S, De Gregorio R, De Sanctis C, Lahti L, Perrone-Capano C, Ponti D, di Porzio U, Perlmann T, Caiazzo M, Volpicelli F, Bellenchi GC (2022) Lmx1a-dependent activation of miR-204/211 controls the timing of Nurr1-mediated dopaminergic differentiation. Int J Mol Sci 23:6961.

Ran FA, Hsu PD, Lin CY, Gootenberg JS, Konermann S, Trevino AE, Scott DA, Inoue A, Matoba S, Zhang Y, Zhang F (2013) Double nicking by RNA-guided CRISPR Cas9 for enhanced genome editing specificity. Cell 154:1380–1389.

Rajman M, et al. (2017) A microRNA-129-5p/Rbfox crosstalk coordinates homeostatic downscaling of excitatory synapses. EMBO J 36:1770–1787.

Reichenstein I, et al. (2019) Human genetics and neuropathology suggest a link between miR-218 and amyotrophic lateral sclerosis pathophysiology. Sci Transl Med 11:eaav5264.

Sawamoto K, Nakao N, Kobayashi K, Matsushita N, Takahashi H, Kakishita K, Yamamoto A, Yoshizaki T, Terashima T, Murakami F, Itakura T, Okano H (2001) Visualization, direct isolation, and transplantation of midbrain dopaminergic neurons. Proc Natl Acad Sci USA 98:6423–6428.

Swahari V, Nakamura A, Hollville E, Stroud H, Simon JM, Ptacek TS, Beck MV, Flowers C, Guo J, Plestant C, Liang J, Kurtz CL, Kanke M, Hammond SM, He YW, Anton ES, Sethupathy P, Moy SS, Greenberg ME, Deshmukh M (2021) MicroRNA-29 is an essential regulator of brain maturation through regulation of CH methylation. Cell Rep 35:108946.

Szklarczyk D, Franceschini A, Wyder S, Forslund K, Heller D, Huerta-Cepas J, Simonovic M, Roth A, Santos A, Tsafou KP (2014) STRING v10: protein–protein interaction networks, integrated over the tree of life. Nucleic Acids Res 43:447–452.

Tan CL, Plotkin JL, Venø MT, von Schimmelmann M, Feinberg P, Mann S, Handler A, Kjems J, Surmeier DJ, O'Carroll D, Greengard P, Schaefer A (2013) MicroRNA-128 governs neuronal excitability and motor behavior in mice. Science 342:1254–1258.

Torres-Berrío A, Nouel D, Cuesta S, Parise EM, Restrepo-Lozano JM, Larochelle P (2018) miR-218: a molecular switch and potential biomarker of susceptibility to stress. Mol Psychiatry 25:951–964.

Torres-Berrío A, Hernandez G, Nestler EJ, Flores C (2020) The Netrin-1/DCC Guidance Cue Pathway as a Molecular Target in Depression: Translational Evidence. Biol Psychiatry 88:611–624.

Volpicelli F, De Gregorio R, Pulcrano S, Perrone-Capano C, di Porzio U, Bellenchi GC (2012) Direct regulation of Pitx3 expression by Nurr1 in culture and in developing mouse midbrain. PLoS One 7:e30661.

Volpicelli F, Speranza L, Pulcrano S, De Gregorio R, Crispino M, De Sanctis C, Leopoldo M, Lacivita E, di Porzio U, Bellenchi GC, Perrone-Capano C (2019) The microRNA-29a modulates serotonin 5-HT7 receptor expression and its effects on hippocampal neuronal morphology. Mol Neurobiol 56:8617–8627.

Yan B, Hu Z, Yao W, Le Q, Xu B, Liu X, Ma L (2017) miR-218 targets MeCP2 and inhibits heroin seeking behavior. Sci Rep 7:40413.

Ying QL, Stavridis M, Griffiths D, Li M, Smith A (2003) Conversion of embryonic stem cells into neuroectodermal precursors in adherent monoculture. Nat Biotechnol 21:183–186.

Yuhao C, Xiaowei W (2020) miRDB: an online database for prediction of functional microRNA targets. Nucleic Acids Research 48:D127–D131.

Wan QF, Zhou ZY, Thakur P, Vila A, Sherry DM, Janz R, Heidelberger R (2010) SV2 acts via presynaptic calcium to regulate neurotransmitter release. Neuron 66:884–895.

Wilkinson DG (1992) Whole mount in situ hybridization of vertebrate embryos. In: In situ hybridization: a practical approach. Oxford: Oxford UP.

Wolfart J, Roeper J (2002) Selective coupling of T-type calcium channels to SK potassium channels prevents intrinsic bursting in dopaminergic midbrain neurons. J Neurosci 22:3404–3413.

Zhao S, Maxwell S, Jimenez-Beristain A, Vives J, Kuehner E, Zhao J, O'Brien C, de Felipe C, Semina E, Li M (2004) Generation of embryonic stem cells and transgenic mice expressing green fluorescence protein in midbrain dopaminergic neurons. Eur J Neurosci 19:1133–1140.